

Taylor & Francis
Taylor & Francis Group

Australian Journal of Earth Sciences

An International Geoscience Journal of the Geological Society of Australia

ISSN: 0812-0099 (Print) 1440-0952 (Online) Journal homepage: www.tandfonline.com/journals/taje20

Adakitic Permian magmatism along the eastern Gondwana margin: constraints on deep crustal processes and metallogenesis in northeastern Queensland

J. Lee, I. V. Sanislav, H. A. Cocker, A. A. Kumar & M. Sami

To cite this article: J. Lee, I. V. Sanislav, H. A. Cocker, A. A. Kumar & M. Sami (14 Oct 2026): Adakitic Permian magmatism along the eastern Gondwana margin: constraints on deep crustal processes and metallogenesis in northeastern Queensland, Australian Journal of Earth Sciences, DOI: 10.1080/08120099.2026.2729731

To link to this article: https://doi.org/10.1080/08120099.2026.2729731

© 2026 The Author(s). Published by Informa UK Limited, trading as Taylor & Francis Group

View supplementary material

Published online: 14 Oct 2026.

Submit your article to this journal

View related articles

View Crossmark data

Full Terms & Conditions of access and use can be found at
https://www.tandfonline.com/action/journalInformation?journalCode=taje20

AUSTRALIAN JOURNAL OF EARTH SCIENCES
https://doi.org/10.1080/08120099.2026.2729731

OPEN ACCESS Check for updates

Adakitic Permian magmatism along the eastern Gondwana margin: constraints on deep crustal processes and metallogenesis in northeastern Queensland

J. Lee[a], I. V. Sanislav[a], H. A. Cocker[a], A. A. Kumar[a#] and M. Sami[b]

[a]Economic Geology Research Centre (EGRU) and Department of Earth and Environmental Sciences, James Cook University, Townsville, QLD, Australia; [b]Geosciences Department, College of Science, United Arab Emirates University, Al Ain, United Arab Emirates

ABSTRACT

The Kennedy Igneous Association (KIA) of northeastern Queensland provides an opportunity to investigate links between granitoid magmatism, deep crustal processes and metallogenesis along the eastern Gondwana margin. This study integrates whole-rock geochemistry with new zircon U–Pb geochronology to constrain the timing, sources and tectonic significance of granitoids from the Georgetown region (Kidston subprovince). Igneous rocks are divided into a Permian group and a Carboniferous group. Zircon U–Pb ages define two principal magmatic episodes: early Carboniferous magmatism (360–333 Ma) and Permian igneous association (296–285 Ma). One intrusion in this study (Mount Darcy; *ca* 375 Ma) pre-dates the KIA and is attributed to older Pama magmatism. Whole-rock geochemistry shows that most samples from the Permian group are characterised by high Sr/Y and $(La/Yb)_N$ together with low Y and Yb, defining a consistent adakitic affinity, whereas the Carboniferous group lacks these signatures. Petrogenetic constraints exclude low-silica adakite, magma mixing and slab-melt models, and instead favour partial melting of lower continental crust under garnet ± amphibole-stable conditions. This melting may have been related to crustal thickening and/or delamination during Carboniferous–Permian convergence along the Gondwana margin. Permian adakitic intrusions temporally overlap recognised mineralisation corridors in the Georgetown region. Although whole-rock fertility proxies alone are not diagnostic, the timing and geochemical character identify Permian magmatism as a priority target for evaluating potential genetic links to Cu–Au mineralisation using independent mineralisation and alteration constraints.

KEY POINTS

1. Zircon U–Pb ages define Permian and Carboniferous magmatic pulses in northeast Queensland.
2. Permian intrusions show adakitic affinity: high Sr/Y and $(La/Yb)_N$ and low Y–Yb and petrogenetic constraints favour lower-crustal melting over slab-derived adakite.
3. Permian adakitic magmatism reflects deep crustal processes on the Gondwana margin.
4. Permian granodiorites overlap mineralised corridors, indicating Cu–Au fertility.

ARTICLE HISTORY
Received 11 May 2026
Accepted 31 August 2026

KEYWORDS
Kennedy Igneous Association; Permian magmatism; lower-crustal melting; Gondwana margin; adakitic magmatism; Cu–Au fertility

Introduction

Granitic magmatism is widely recognised as a fundamental driver of many hydrothermal ore systems, because evolving magmas supply heat, fluids and metals to the upper crust (Hedenquist & Lowenstern, 1994; Richards, 2011). Porphyry Cu(–Au) deposits, in particular, are genetically and temporally linked to intermediate–felsic intrusions and their magmatic–hydrothermal evolution (Seedorff *et al*., 2005; Sillitoe, 2010). Adakites were originally defined as intermediate to felsic rocks characterised by high Sr/Y and $(La/Yb)_N$ ratios and low Y and Yb contents and were genetically attributed to melting of young subducted oceanic crust (Defant & Drummond, 1990). Irrespective of their specific origin, granitoids with high Sr/Y signatures have been suggested to play a significant role in magmatic–hydrothermal Cu and/or Au mineralisation, because these signatures may reflect oxidised, water-rich conditions favourable for porphyry Cu(–Au) fertility (Loucks, 2014). However, similar adakitic geochemical signatures can be generated by processes other than slab melting, and ore-bearing examples formed through alternative petrogenetic processes have also been reported (Hu *et al*., 2015; Wang *et al*., 2007).

Multiple tectonic settings and petrogenetic processes have been proposed for adakites and adakitic rocks, including slab melting, melt–mantle interaction, melting of overthickened lower continental crust, delamination-related melting and magma mixing and/or assimilation (Atherton & Petford, 1993; Defant & Drummond, 1990; Gao *et al*., 2004; Kawaguchi *et al*., 2023; Streck *et al*., 2007). Regardless of tectonic setting, these geochemical signatures are ultimately controlled by the mineral

CONTACT Jonghyun Lee jonghyun.lee@my.jcu.edu.au Economic Geology Research Centre (EGRU) and Department of Earth and Environmental Sciences, James Cook University, Townsville, QLD 4811, Australia
[#]Present Address: University College Dublin, School of Earth Sciences, Belfield, Dublin 4, Ireland
Supplemental data for this article can be accessed online at https://doi.org/10.1080/08120099.2026.2729731.
Editorial handling: Chris Fergusson
© 2026 The Author(s). Published by Informa UK Limited, trading as Taylor & Francis Group
This is an Open Access article distributed under the terms of the Creative Commons Attribution License (http://creativecommons.org/licenses/by/4.0/), which permits unrestricted use, distribution, and reproduction in any medium, provided the original work is properly cited. The terms on which this article has been published allow the posting of the Accepted Manuscript in a repository by the author(s) or with their consent.

assemblages involved in source partial melting and subsequent magmatic evolution, particularly the presence or absence of garnet, amphibole and plagioclase. In several provinces, however, the tectonic setting responsible for adakitic rocks remains difficult to constrain and their origin remains debated, underscoring the need for integrated geochemistry and robust geochronology. In north Queensland, recent recognition of diamond-facies ultrahigh-pressure metamorphism along the Clarke River Fault demonstrates that parts of the northern Tasmanides record deep continental subduction and collisional tectonics, rather than purely accretionary margin processes, fundamentally changing constraints on crustal thickness and melt sources during Paleozoic magmatism (*e.g.* Edgar *et al*., 2022).

Carboniferous–Permian magmatism in northeastern Australia developed along the eastern margin of Gondwana during a prolonged interval of convergent margin evolution associated with the northern Tasmanides (Withnall & Henderson, 2012). This margin records complex tectonic behaviour, including long-lived subduction, episodic crustal thickening, slab rollback and tectonic switching between contractional and extensional regimes, which collectively influenced magma sources, storage depths and metallogenic fertility (Blevin, 2004; Blevin *et al*., 1996; Cheng *et al*., 2018). Understanding how these Gondwana-margin processes controlled the generation of compositionally diverse granitoid magmas, including adakitic variants, is therefore critical for reconstructing the tectono-magmatic architecture of northeastern Australia and assessing its mineralisation potential. Against this backdrop, linking adakitic geochemical signatures to specific mineralisation pulses is particularly challenging in regions where multiple Paleozoic magmatic episodes overlap. Mafic–ultramafic complexes and adakitic felsic plutons aligned with major Paleozoic fault systems in northeast Queensland have been interpreted as fragments of supra-subduction zone lithosphere and continental-arc magmatism associated with long-lived suture zones in the northern Tasmanides (Edgar *et al*., 2022, 2023). Detailed geochronological, geochemical and structural studies from the Running River Metamorphics demonstrate that the northeastern Thomson Orogen formed in a long-lived continental arc to collisional setting during the early Paleozoic, reflecting continuous convergence along the paleo-Pacific margin of Australia (Dirks *et al*., 2021). The Georgetown region of northeastern Queensland, part of the Kennedy Igneous Association (KIA), provides an ideal setting to examine these relationships. High Sr/Y adakitic signatures in the Georgetown region have not been systematically evaluated or reported previously, although elevated Sr contents in some Permian granitoid rocks have been noted (Champion & Bultitude, 2013b). In addition, two mineralisation epochs have been recognised in the KIA: an early Carboniferous intrusion-related gold system (the Kidston deposit) and a late Carboniferous to early Permian intrusion-related and epithermal gold–silver system (Mount Turner and Log Creek deposits) in the Georgetown region (Morrison *et al*., 2019). These observations raise the possibility that Permian magmatism in the Georgetown region may include previously unrecognised adakitic signatures, with implications for porphyry-style Cu(–Au) fertility. In the broader KIA, Carboniferous–Permian magmatism is demonstrably linked to magmatic–hydrothermal Sn–Cu–In systems, with mineralisation pulses tightly constrained between *ca* 320 and 280 Ma, indicating that fertile magmas and efficient metal transfer systems were active during this interval (Kumar *et al*., 2022, 2023).

In this paper, we present whole-rock major- and trace-element data (XRF and ICP-OES/ICP-MS) together with new LA-ICP-MS zircon U–Pb geochronology for Permian granitoids in the Georgetown region of northeastern Queensland that may be spatially and temporally associated with porphyry-style Cu(–Au) mineralisation. We also compare these granitoids with Carboniferous granitoids from the same region to constrain temporal variations in magma chemistry and source characteristics. We further evaluate the significance of adakitic signatures in relation to Permian porphyry Cu(Au) fertility and discuss the tectonic setting that generated adakitic magmas during the Permian.

Geological setting

KIA

The KIA (Bain & Draper, 1997) comprises widespread and voluminous intrusive and extrusive rocks dominated by silicic and evolved magmatism across northern Queensland during the Carboniferous to Permian (*ca* 340–270 Ma; Figure 1a). The KIA forms a discontinuous belt of plutons, hypabyssal porphyry systems, dykes and felsic volcanic fields emplaced into Proterozoic and Paleozoic basement provinces. The plutons are composed mainly of I-type granitoids, with subordinate S-type and minor A-type, and are characterised by high SiO_2, K and LILE contents (Bultitude & Champion, 1992; Champion, 1994; Mackenzie & Wellman, 1997).

The KIA is considered to continue northward from the New England Orogen as a north-northwest-trending magmatic belt. Geophysical data define the Townsville-Mornington Island Belt (TMIB), which is interpreted as part of the KIA; the TMIB is concealed between Mount Surprise and Mornington Island (Wellman, 1992, 1995; Wellman *et al*., 1994) and extends west-northwest. Although its origin has been debated, the TMIB contains batholiths, smaller intrusions and numerous volcanic fields, many of which are cauldron complexes with piles of dacitic–rhyolitic ignimbrites (Bultitude *et al*., 1997; Mackenzie & Wellman, 1997; Withnall *et al*., 1997; Withnall & Henderson, 2012).

Previous studies typically suggest that the KIA developed along a west-dipping active continental margin (Withnall & Henderson, 2012). Cheng *et al*. (2018) and Withnall and Henderson (2012) recognised two main stages of KIA emplacement. Early Carboniferous magmatism is interpreted to reflect partial melting of crustal sources during crustal thickening. This was followed, from the late Carboniferous to early Permian, by crustal melting driven by basaltic underplating during slab rollback (Champion & Bultitude, 2013a; Mackenzie & Wellman, 1997; Murgulov *et al*., 2007). This later stage has been interpreted to reflect extension within an active subduction setting, involving changes in slab angle, back-arc rifting and rollback. The TMIB, in particular, may represent a cauldron system formed within a complex rift system during extension related to slab retreat (Withnall *et al*., 1997; Withnall & Henderson, 2012).

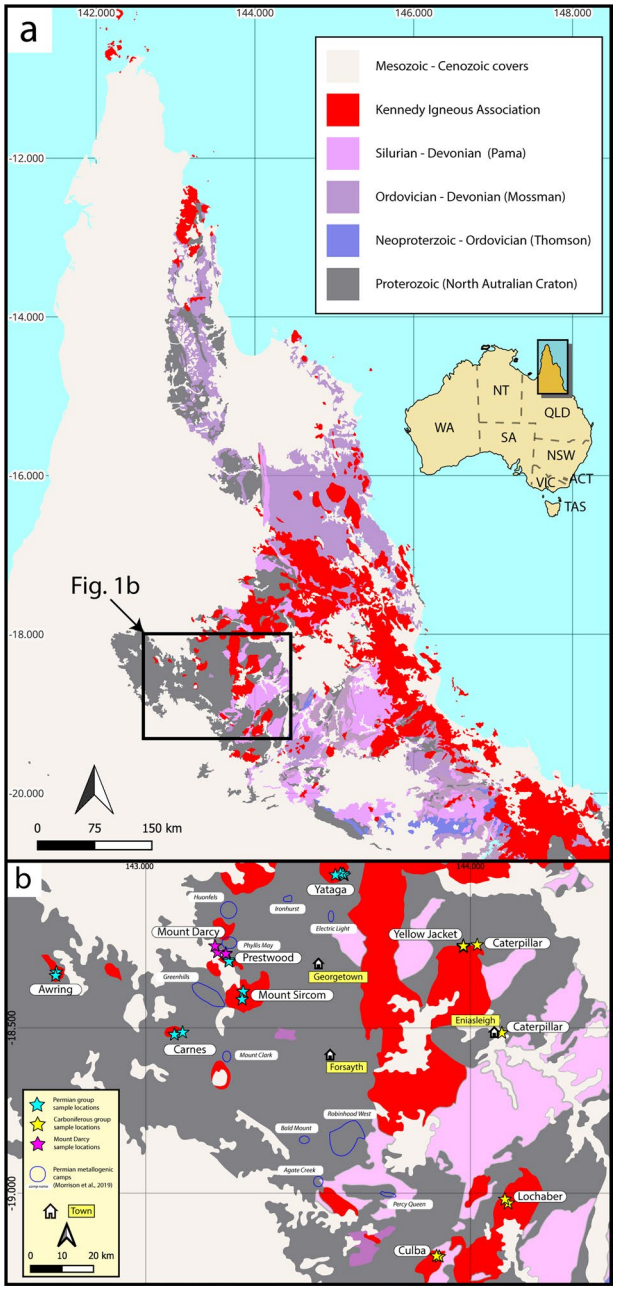


Figure 1. Regional distribution of the Kennedy Igneous Association and sample locations in the Georgetown region (Kidston subprovince), northeastern Queensland. (a) Simplified geological map of northeastern Queensland showing the distribution of the Kennedy Igneous Association and surrounding tectonostratigraphic provinces. (*e.g.* North Australian Craton, Thomson Province, Mossman Orogen, Pama Igneous Association) and younger sedimentary cover. The black rectangle indicates the area enlarged in (b). (b) Detailed geological map around Georgetown showing sample sites (stars) and analysed intrusion/volcanic units. Major towns are labelled for reference (*e.g.* Georgetown, Forsayth, Einasleigh) and showing the spatial relationship between the Permian group intrusions, sample locations and Permian metallogenic camps in the Georgetown region. Permian camp outlines are after Morrison *et al.* (2019).

KIA in the Georgetown region (the Kidston subprovince)

Carboniferous–Permian magmatism in the Kidston subprovince comprises ~40% intrusive rocks (~1200 km^2) and ~60% extrusive rocks (~1900 km^2). Magmatism is predominantly high-level and shallow, as indicated by widespread volcanic and subvolcanic to epizonal rocks with locally common miarolitic cavities (Champion & Bultitude, 2013b). Magmatism spans *ca* 345–280 Ma (Fanning, 1996; Murgulov *et al.*, 2009; Withnall *et al.*, 1997) and is episodic, with two main pulses in the Carboniferous (*ca* 345–335 Ma) and Permian (*ca* 290–280 Ma; Withnall *et al.*, 1997).

Most I-type granitoid units in the Kidston subprovince have not been formally defined, despite their wide distribution. Some I-type intrusions are associated with the Kidston Au–Mo–Bi deposit (Glenmore Supersuite), with emplacement ages constrained at 340–338 Ma (Baker & Andrew, 1991; Blevin & Morrison, 1997) and other Au–Pb–Zn occurrences with small porphyry-type Cu prospects and minor Cu mineralisation (Mackenzie & Wellman, 1997). Relatively young Permian intrusions have also been reported in the western Georgetown region.

In contrast, Permian A-type magmatism forms a relatively small component of the subprovince and is largely confined to small high-level intrusions associated with the Eveleigh and Namarrong volcanic subgroups of the Newcastle Range Volcanic Group (Champion, 1994; Oversby & McKenzie, 1994). A-type intrusions are more abundant than their extrusive equivalents. Volcanic rocks are widespread across the Kidston subprovince, with the Newcastle Range Volcanic Group being the most extensive unit. It comprises ~85–90% rhyolite and ~5–10% dacite, and includes rhyolitic ignimbrite, lavas and tuffs (Champion & Bultitude, 2013b).

Mineralisation related to the KIA (Kidston subprovince)

Although mineralisation in the Kidston subprovince is relatively sparse, I-type intrusions of the KIA are associated with the Kidston Au–Mo–Bi deposit, a major gold producer in Queensland (Champion & Bultitude, 2013b). Morrison *et al.* (2019) reported three Paleozoic mineralisation periods in the Georgetown region, two of which are related to the KIA: (i) an early Carboniferous intrusion-related Au group (350–320 Ma) and (ii) a late Carboniferous to early Permian intrusion-related and epithermal Ag–Au group (320–270 Ma).

The early Carboniferous group includes scattered mineral occurrences in the Einasleigh Metamorphics along the eastern side of the Newcastle Range. These occurrences, including the Kidston deposit as a representative example, comprise mesozonal–epizonal hydrothermal breccias and vein networks associated with rhyolite plugs and dykes. The late Carboniferous to early Permian group comprises two distinctive corridors: one in the northwest of Georgetown extending from the Robertson Fault through the Ag–Cu Phyllis May and Red Dam prospects towards Chillagoe, and another extending southeast along the Robertson Fault through the Ag–Au Agate Creek deposit. Mineralisation includes Ag-rich polymetallic stockwork and breccia mineralisation at the Phyllis May prospect and Ag–Au epithermal deposits associated with rhyolitic dykes. The Mt. Turner and Log Creek Ag–Au deposits are also associated with late Carboniferous subvolcanic intrusions within this broader mineralisation interval. This metallogenic framework provides a basis for assessing whether Permian granitoids in the

Georgetown region record adakitic signatures and whether these features coincide with conditions favourable for porphyry-style Cu(–Au) fertility.

Samples and methodology

Samples

Fieldwork was undertaken in the Georgetown region to collect igneous rock samples of the KIA. Samples were collected and grouped primarily by emplacement age into: (i) a Permian group, comprising the Yataga, Awring, Carnes and Mount Sircom granodiorite–tonalite intrusions and the Prestwood granite; and (ii) a Carboniferous group, comprising the Caterpillar, Lochaber and Culba granites and the Yellow Jacket Rhyolite (Figure 1b). A summary of samples, analyses and key characteristics is provided in Table 1, and hand-specimen textures are briefly summarised below. Mount Darcy was initially sampled as part of the KIA, but zircon U–Pb dating in this study indicates a significantly older age (*ca* 375 Ma); it is therefore treated separately as a pre-KIA outlier.

Whole-rock geochemistry

Whole-rock geochemical data, including major, trace and rare earth element (REE) concentrations, were obtained from Bureau Veritas Commodities Canada Ltd (Vancouver, BC, Canada). Representative rock samples were submitted to Bureau Veritas for sample preparation and analysis. At Bureau Veritas, samples were crushed to 70% passing 2 mm and then pulverised to <75 µm. The powdered samples were analysed using a lithium borate fusion with X-ray fluorescence for major elements and selected minor elements (BV code XF700) and ICP-OES/ICP-MS analyses for trace elements (BV code LF100-EXT). Major- and trace-element geochemical data are provided in the Supplemental data (Table S1).

Zircon U–Pb geochronology

Nine representative samples were selected for zircon U–Pb analysis, prioritising the freshest sample from each unit; units with existing robust geochronological constraints were generally not re-analysed. Nine samples were crushed and then milled and sieved to a grainsize of <500 µm. Heavy minerals were separated from the sieved fractions using a Wilfley table and a portable magnet. Zircon grains were hand-picked from the heavy mineral separates under a binocular microscope, and selected grains were mounted in epoxy resin and polished to near mid-section exposure. To identify zoning patterns, back-scattered electron and cathodoluminescence (CL) images were obtained using a JEOL JSM5410LV scanning electron microscope at the Advanced Analytical Centre (AAC), James Cook University (JCU), Australia.

The zircons were analysed for U–Pb isotopes with an Analyte G2 Excimer Laser Ablation system coupled to a Thermo iCap-RQ ICP-MS instrument. The ablation was carried out at an energy density of 2 J/cm^2, a repetition rate of 5 Hz, and a spot size of 25 µm at the AAC, JCU. Isotope data reduction was carried out using Iolite (Fisher *et al*., 2017). Mean age values were selected based on a < 5% discordance between the $^{206}Pb/^{238}U$ and $^{207}Pb/^{235}U$ ages, and age calculations were performed with IsoplotR (Vermeesch, 2018). Weighted mean ages were calculated using the $^{206}Pb/^{238}U$ isotope system. Unless otherwise stated, uncertainties for individual analyses and calculated sample ages are reported at the 2σ level. For igneous samples, more than 50 zircon spots were analysed from each unit and only results within 5% discordance were used to calculate ages. The primary standard used for downhole fractionation corrections was the Plesovice zircon (ID-TIMS $^{206}Pb/^{238}U$ age of 337.13 ± 0.37; Sláma *et al*., 2008). Zircon standards GJ-1 (ID-TIMS $^{207}Pb/^{206}Pb$ age of 608 ± 1 Ma and $^{206}Pb/^{238}U$ age of 602 ± 0.4 Ma; Horstwood *et al*., 2016; Jackson *et al*., 2004) and 91500 ($^{207}Pb/^{206}Pb$ age of 1067 ± 1.5 Ma and $^{206}Pb/^{238}U$ age of 1064 ± 0.65 Ma; Horstwood *et al*., 2016; Wiedenbeck *et al*., 1995) were used as the secondary zircon standards. U–Pb isotope data are provided in the Supplemental data (Table S2).

Results

Petrography

Permian group

The Permian group intrusions are dominantly granodiorite–tonalite and show porphyritic to medium–coarse-grained textures. Within the Yataga intrusion, less fractionated samples collected from the intrusion margin comprise weakly foliated granodiorite to tonalite (Figure 2a), whereas more fractionated

Table 1. Summary of representative samples, analytical coverage and key geochemical–geochronological characteristics of the Georgetown granitoids.

		Whole rock		Geochronology			Location (representative)	
Granitoid units	Group	n	Sr/Y (mean)	Age (Ma)		n (concordia)	Latitude	Longitude
Yataga (less fractionated rim part)	Permian	3	36	280	Jell (2013)		−18.044203	143.626835
Awring	Permian	2	52	285±5	This study	8	−18.347979	142.754671
Mount Sircom 26	Permian	2	101	288±5	This study	19	−18.395852	143.321319
Mount Sircom 29	Permian	1	104	292±4	This study	26	−18.419757	143.318263
Prestwood	Permian	2	2	296±4	This study	20	−18.304960	143.278346
Carnes	Permian	2	33	294±3	This study	20	−18.525911	143.113290
Lochaber	Carboniferous	2	2	333±6	This study	5	−19.024251	144.112296
Culba	Carboniferous	2	16	360±2	This study	24	−19.197311	143.913891
Yellow Jacket	Carboniferous			339±2	This study	19	−18.261541	143.986787
Caterpillar	Carboniferous			335±2	This study	28	−18.254791	144.028726
Mount Darcy	Devonian	4	87	375±2	This study	25	−18.280427	143.268963

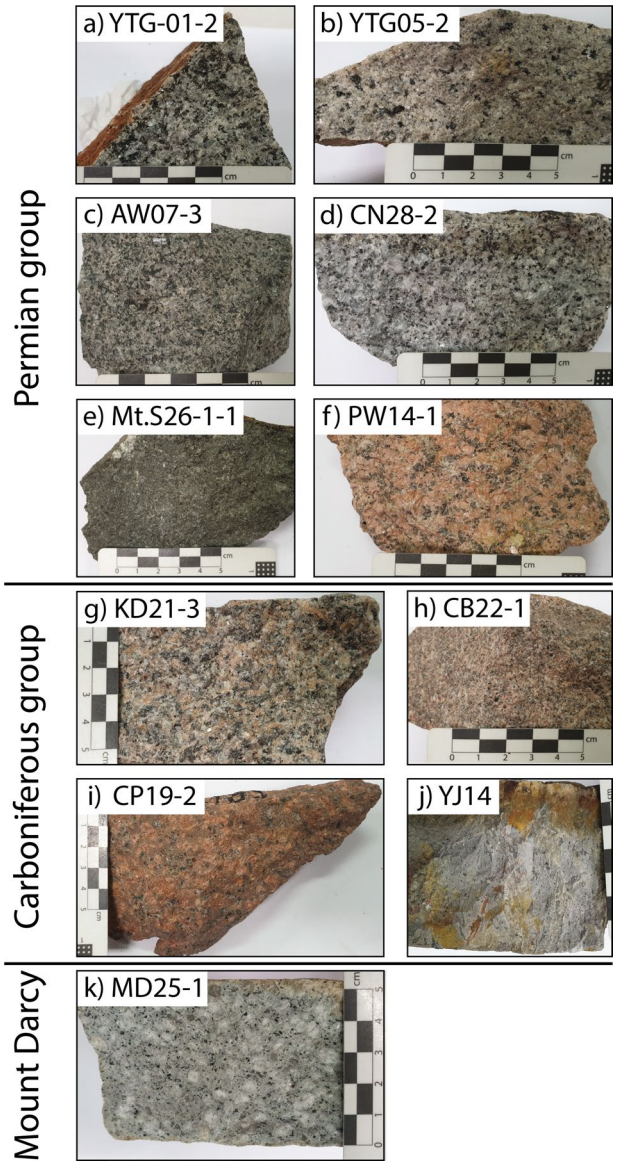


Figure 2. Representative hand-specimen photographs of the Permian and Carboniferous groups from the Georgetown region. Permian group samples are shown in (a–f) and Carboniferous group samples in (g–j). Scale bars in centimetres. (a) Rim part of the Yataga intrusion (YTG01-2). (b) Core part of the Yataga intrusion (YTG05-2). (c) Awring Granodiorite (AW07-3). (d) Carnes Granodiorite (CN28-2). (e) Mount Sircom Granodiorite (Mt.S 26-1). (f) Prestwood Granite (PW14-1). (g) Lochaber Granite (KD21-2). (h) Culba Granite (CB22-1). (i) Caterpillar Granite (CP19-2). (j) Yellow Jacket Rhyolite (YJ 14). (k) Mount Darcy Granodiorite (MD 25-1).

samples from its central part comprise porphyritic granodiorite to granite. Both domains are mainly composed of plagioclase (40–50 vol%), quartz (30–40 vol%) and variable amphibole and biotite (together ~20 vol%; Figure 2b). Samples from the intrusion margin contain oscillatory-zoned plagioclase, greenish biotite and amphibole, with acicular and hexagonal apatite occurring as inclusions in mafic minerals (Figure 3a). Samples from the central part also contain oscillatory-zoned plagioclase and coarse brownish biotite, with apatite inclusions in quartz and biotite and zircon inclusions in biotite; graphic textures and interstitial biotite between quartz grains are locally present (Figure 3b). The Awring Granodiorite is porphyritic with plagioclase phenocrysts in a quartz-rich matrix (Figure 3c), and some samples contain sulfides visible in hand specimen. Plagioclase locally contains apatite inclusions, and quartz is typically anhedral and locally forms graphic intergrowths. The Carnes Granodiorite is medium- to coarse-grained and comprises plagioclase (~40 vol%) and quartz (~40 vol%) but lacks amphibole (Figure 2d); biotite is greenish-brown and both plagioclase and biotite commonly host apatite and/or zircon inclusions (Figure 3d). The Mount Sircom Granodiorite is a grey, porphyritic intrusion with needle-shaped amphibole; samples comprise plagioclase, quartz and amphibole, with plagioclase as the main phenocryst phase and a quartz-rich groundmass (Figures 2e and 3e). Amphibole is typically pale green with weak alteration, apatite inclusions occur locally, and zircon inclusions are observed in some amphibole and plagioclase grains. Antiperthite exsolution features occur in some albite grains.

The Prestwood Granite is described separately below because it is strongly altered and petrographically distinct from the granodiorite–tonalite intrusions. The Prestwood Granite (PW) is a pink-coloured, coarse-grained (alkali-) granite comprising quartz (50–60 vol%), plagioclase (~30 vol%), alkali feldspar (10–20 vol%) and biotite (~5 vol%) (Figure 2f). However, it has been strongly altered, such that primary quartz is largely preserved, whereas biotite is chloritised and feldspars are sericitised. Microscopic observations reveal graphic textures, rounded quartz grains and biotite infilling interstitial spaces between quartz and alkali feldspar grains (Figure 3f).

Carboniferous group

The Lochaber Granite (KD) can be subdivided into fine–medium-grained and medium-grained varieties based on grainsize, although both have similar mineral assemblages (Figure 2g). It comprises quartz (~25 vol%), alkali feldspar (~50 vol%), plagioclase (~20 vol%) and brownish biotite (~5 vol%) (Figure 3g), and some samples contain secondary muscovite. The Culba Granite (CB) is a grey to pink, fine- to medium-grained granite (Figure 2h) comprising quartz (~50 vol%), alkali feldspar (~25 vol%), plagioclase (~20 vol%) and brown biotite (~5 vol%); it is strongly altered with sericitised alkali feldspar and chloritised biotite (Figure 3h). The Caterpillar Granite (CP) is a reddish, coarse-grained granite (Figure 2i) dominated by alkali feldspar (~60 vol%) and plagioclase (~30 vol%), with minor quartz (~10 vol%) and trace chloritised biotite (~1 vol%), and quartz grains are typically rounded. The Yellow Jacket (YJ) Rhyolite has a light to dark grey matrix and locally contains sulfide minerals such as pyrite (Figure 2j); phenocrysts are dominated by feldspar with minor quartz, and fiamme textures are observed.

Mount Darcy

The Mount Darcy Granodiorite (MD) consists of a medium-coarse-grained granodiorite and a porphyritic granodiorite (Figure 2k). These two types include plagioclase (40–45 vol%), quartz (40–45 vol%) and mafic minerals (~15 vol%), but the porphyritic type also has visible sulfide minerals in hand specimen.

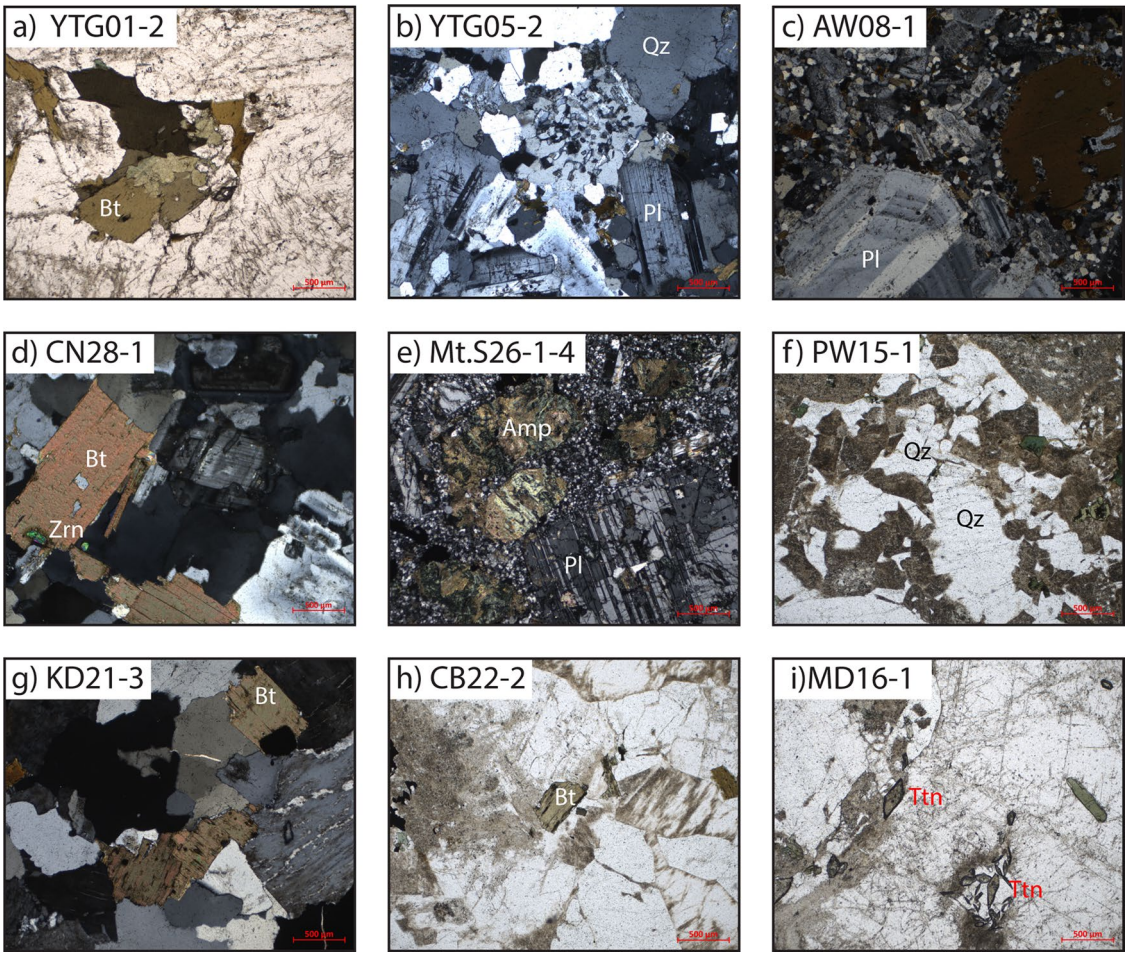


Figure 3. Representative photomicrographs of thin-sections of the Permian and Carboniferous groups (Scale bar = 500 µm in all panels). (a) Rim part of the Yataga intrusion (YTG01-2) (plane-polarised light, PPL); greenish biotite interstitial to quartz and feldspar. (b) Core part of the Yataga intrusion (YTG05-2) (crossed polarised light, XPL); micrographic texture. (c) Awring Granodiorite (AW08-1) (XPL); zoned plagioclase phenocrysts. (d) Carnes Granodiorite (CN28-1) (XPL); plagioclase phenocrysts with zircon inclusions. (e) Mount Sircom Granodiorite (Mt.S 26-1-4) (XPL); amphibole and plagioclase phenocrysts in a quartz-rich groundmass. (f) Prestwood Granite (PW15-1) (PPL); equigranular quartz with strongly altered feldspar. (g) Lochaber Granite (KD21-3) (XPL); equigranular quartz–feldspar–biotite granite. (h) Culba Granite (CB22-2) (PPL); biotite associated with quartz and strongly altered feldspar. (i) Mount Darcy Granodiorite (MD16-1) (PPL); titanite as an accessory phase. Abbreviations: Amp, amphibole; Bt, biotite; Pl, plagioclase; Qz, quartz; Ttn, titanite; Zrn, zircon. Scale bars as shown.

Accessory minerals in both granodiorites include apatite, zircon and titanite. The samples show weak alteration with minor sericite alteration of feldspars and chlorite alteration of biotite (Figure 3i).

Geochemistry

Permian group

Whole-rock major- and trace-element results are presented in the Supplemental data (Table S1). The Permian group is characterised by a wide range of SiO_2 contents (60–75 wt%) (Figure 4) and systematic fractionation trends: TiO_2, Al_2O_3, CaO, Fe_2O_3, MgO and P_2O_5 decrease with increasing SiO_2, whereas K_2O increases; Na_2O shows no clear trend (Figure 4). The Yataga Granodiorite is more fractionated towards the pluton core, and the more fractionated core samples show higher Th and U than other granodiorites.

Within the Permian group, samples are enriched in Ba, Sr and V and depleted in Rb, Y and Nb (Figure 5; Table S1). Sr and V decrease systematically with increasing SiO_2, consistent with progressive fractionation (Figure 5). Chondrite-normalised REE patterns show LREE enrichment and HREE depletion with steep slopes [$(La/Yb)_N = 14.31–49.20$] and weakly negative to positive Eu anomalies (Figure 6a). Primitive mantle-normalised patterns display pronounced Nb–Ta troughs and P–Ti depletions (Figure 6c), with fractionation of plagioclase, apatite and Ti-bearing oxides (*e.g.* ilmenite) inferred from these features. Granodiorite samples are sub-alkaline and range from diorite to granite on the TAS diagram (Figure 7a), span calc-alkaline to high-K calc-alkaline series (Figure 7b), cluster near the metaluminous–peraluminous boundary on the ASI diagram (Figure 7c) and plot predominantly in the VAG field on tectonic discrimination diagrams (Figure 7d).

Carboniferous group

In contrast, the Carboniferous group is more silicic and more fractionated, with lower Ba–Sr–V and higher Rb–Y–Nb, together with flatter REE patterns and pronounced negative Eu

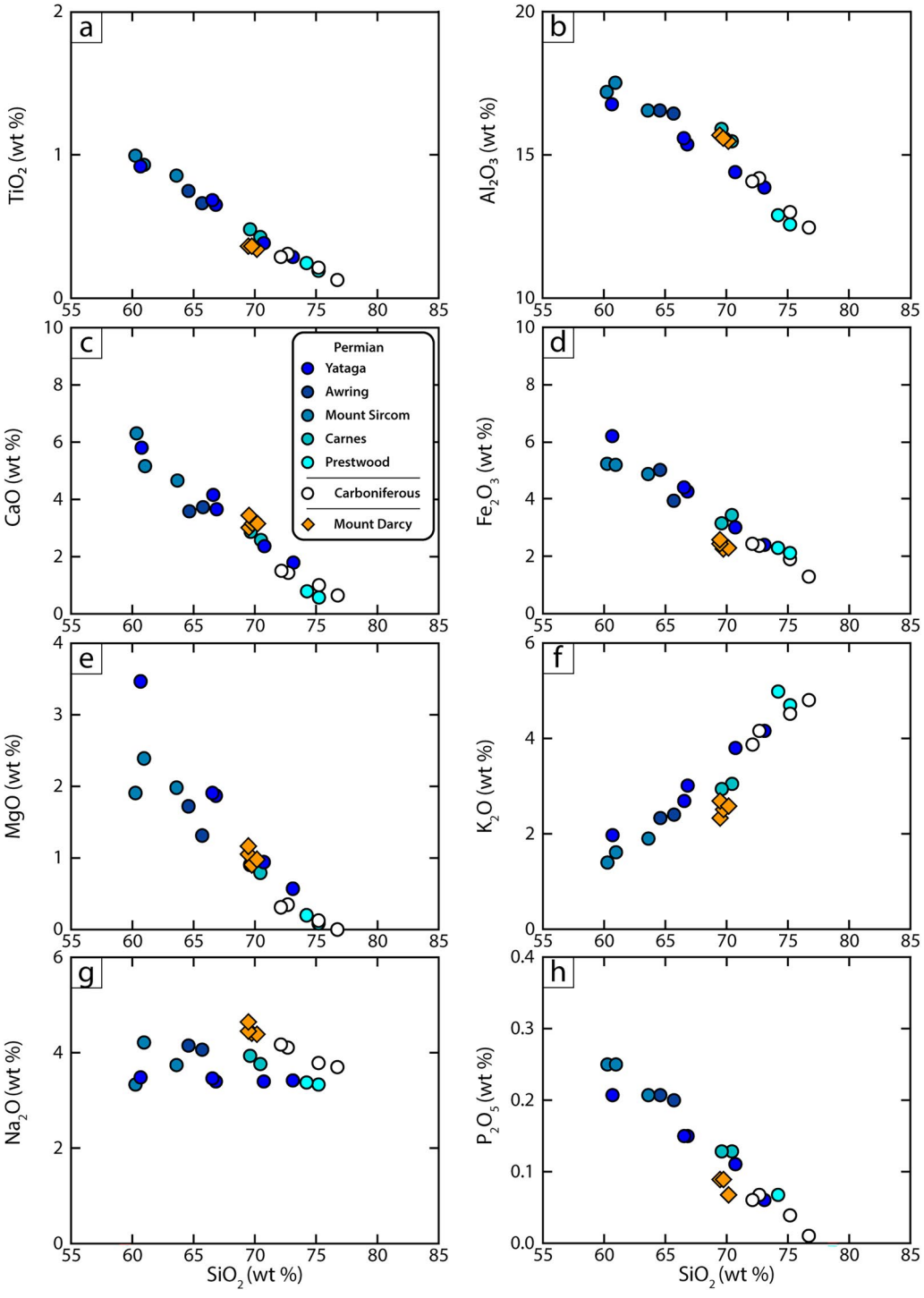


Figure 4. Harker diagrams (wt %) for the Permian group, Carboniferous group and Mount Darcy. (a) TiO_2, (b) Al_2O_3, (c) CaO, (d) Fe_2O_3, (e) MgO, (f) K_2O, (g) Na_2O and (h) P_2O_5 plotted against SiO_2. Symbols: individual Permian intrusive units are distinguished by different shades of blue (filled circles), the Carboniferous group by open circles and Mount Darcy by orange diamonds.

anomalies (Figures 5 and 6; Table S1). The Carboniferous group has overall higher SiO_2 contents than the Permian group and exhibits more fractionated compositions (Figure 4). Although both groups show similar Harker trends, granite–rhyolite samples have lower TiO_2, Al_2O_3, CaO, Fe_2O_3, MgO and P_2O_5 and higher K_2O; Na_2O shows no clear trend and overlaps with the granodiorites (Figure 4). In trace-element space, these samples are depleted in Ba, Sr and V but relatively enriched in Rb, Y and Nb (Figure 5).

REE patterns are flatter and relatively HREE-enriched compared with those of the Permian group [$(La/Yb)_N$ = 3.31–22.34] and show pronounced negative Eu anomalies (Figure 6b); Culba Granite samples have lower overall REE abundances than other Carboniferous units. Primitive mantle-normalised patterns show

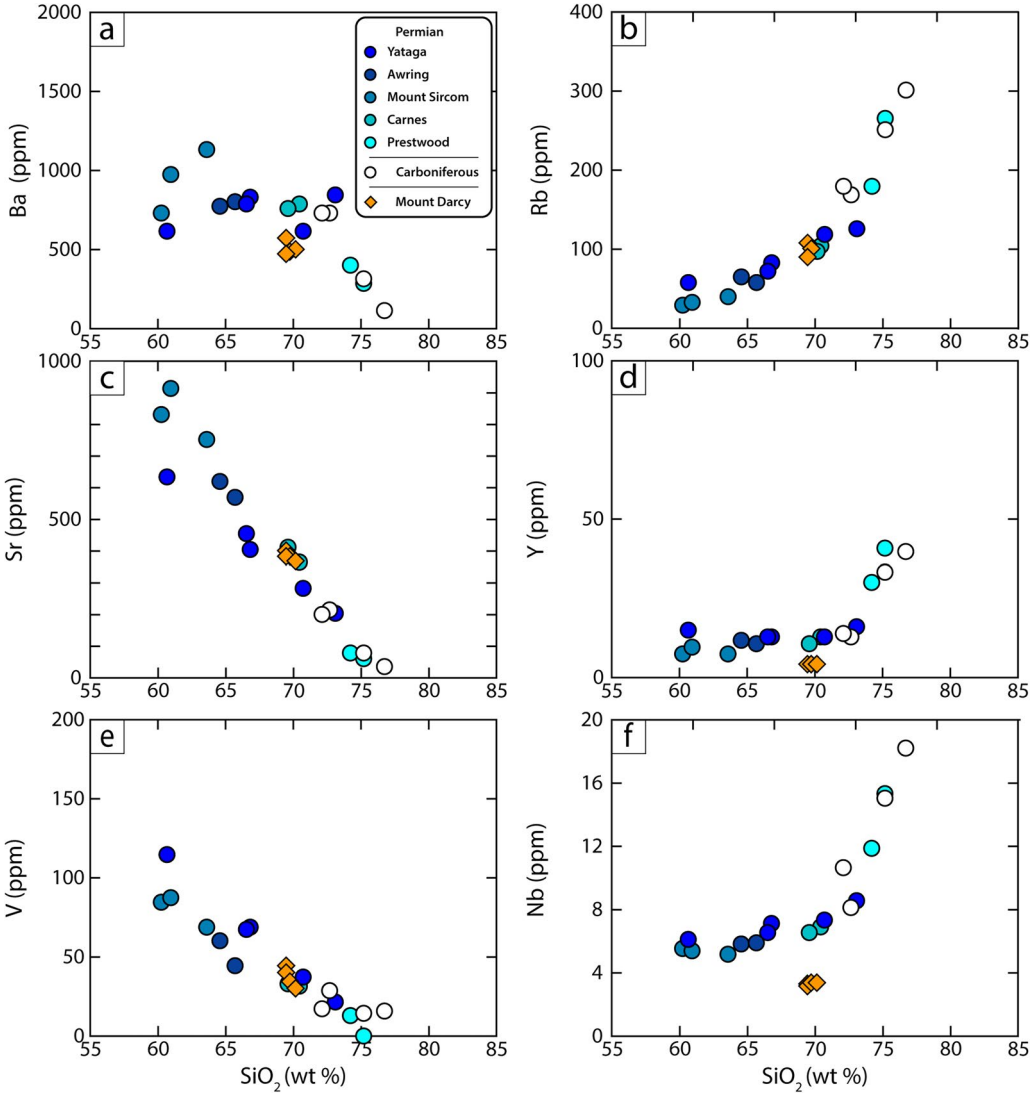


Figure 5. Trace elements plots for the Permian group, Carboniferous group and Mount Darcy. (a) Ba, (b) Rb, (c) Sr, (d) Y, (e) V and (f) Nb (all in ppm). Symbols as in Figure 4.

Nb–Ta troughs and strong Ba–Sr–P–Ti depletions together with Th–U enrichment (Figure 6d). These samples are sub-alkaline and high-K calc-alkaline (Figure 7a, b), are peraluminous with A/CNK generally <1.1 (Figure 7c) and extend from the VAG field into the WPG field on tectonic discrimination diagrams (Figure 7d), reflecting their higher Y, Nb and Rb contents.

Zircon U–Pb geochronology

Permian group

Zircon U–Pb results for the Permian group define a coherent magmatic episode at *ca* 296–285 Ma (Figures 8 and 9). Zircons from AW08 are typically euhedral and show high luminescence with weak concentric zoning (Figure 8a), yielding a concordia age of 285 ± 5 Ma and an identical $^{206}Pb/^{238}U$ weighted mean age (MSWD = 1.3, n = 8; Figure 9a). Zircons from CN28 are elongated and euhedral, with concentric zoning in some grains (Figure 8b) and give a $^{206}Pb/^{238}U$ weighted mean age of 294 ± 3 Ma (MSWD = 1.4, n = 20) with an identical concordia age (Figure 9b). Two Mount Sircom samples (Mt.S26-1 and Mt.S29-1) contain mostly euhedral zircons with moderate to high luminescence and magmatic concentric zoning (Figure 8c, d). Mt.S26-1 yields a $^{206}Pb/^{238}U$ weighted mean age of 288 ± 5 Ma (MSWD = 0.31, n = 19) with an identical concordia age (Figure 9c), whereas Mt.S29-1 yields 292 ± 4 Ma (MSWD = 0.29, n = 26; Figure 9d), overlapping Mt.S26-1 within uncertainty. Zircons from PW15 (Prestwood Granite) are mostly euhedral and show low luminescence with well-defined concentric zoning (Figure 8e); the sample yields a $^{206}Pb/^{238}U$ weighted mean age of 296 ± 4 Ma (MSWD = 0.49, n = 20) with an identical concordia age (Figure 9e), consistent with Permian emplacement.

Carboniferous group

Zircon U–Pb results for the Carboniferous group define an older magmatic episode spanning 360–333 Ma (Figures 8 and 9). Zircons from CB22 (Culba Granite) are predominantly euhedral

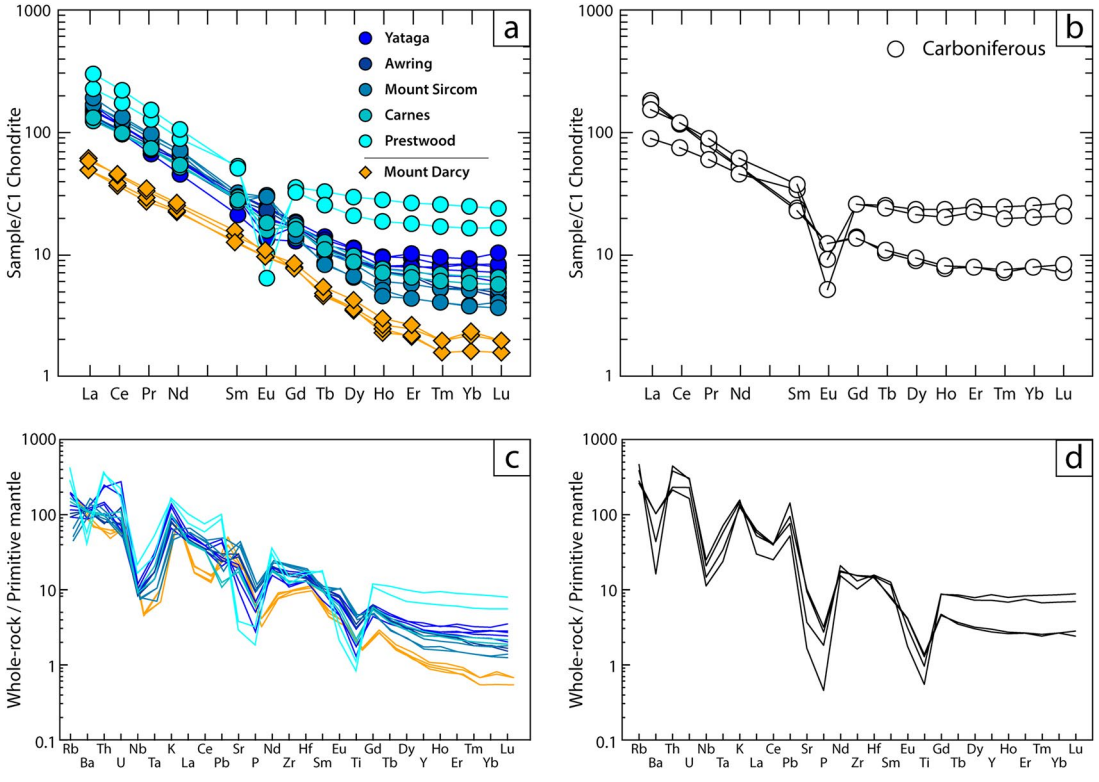


Figure 6. Chondrite-normalised rare earth element diagrams (Sun & McDonough, 1989) and primitive mantle-normalised incompatible element diagrams (McDonough & Sun, 1995) for the Permian group, Carboniferous group and Mount Darcy. (a) Chondrite-normalised REE patterns for the Permian group, with the Mount Darcy sample shown for comparison. (b) Chondrite-normalised REE patterns for the Carboniferous group. (c) Primitive mantle-normalised multi-element patterns for the Permian group, with Mount Darcy plotted separately. (d) Primitive mantle-normalised multi-element patterns for the Carboniferous group.

and show low luminescence with weakly developed concentric zonation (Figure 8f), yielding a concordia age of 360 ± 2 Ma and an identical $^{206}Pb/^{238}U$ weighted mean age (MSWD = 1.8, n = 24; Figure 9f). In CP19 (Caterpillar Granite), zircons are predominantly euhedral; some grains contain mineral inclusions, and many show low luminescence with moderately developed concentric zoning (Figure 8g), yielding a $^{206}Pb/^{238}U$ weighted mean age of 335 ± 2 Ma (MSWD = 2.0, n = 28) with an identical concordia age (Figure 9g). Zircons from KD21 (Lochaber Granite) are commonly euhedral and show low luminescence with concentric zoning (Figure 8h). Only five analyses satisfied the <5% discordance criterion, yielding a $^{206}Pb/^{238}U$ weighted mean age of 333 ± 6 Ma (MSWD = 8.4, n = 5) and a comparable concordia age (Figure 9h). Given the small number of accepted analyses and significant excess scatter, this age is considered tentative rather than a robust emplacement age. In YJ13 (Yellow Jacket Rhyolite), zircons are commonly euhedral, and CL images show low to moderate luminescence with well-defined concentric zoning in most grains (Figure 8i), yielding a $^{206}Pb/^{238}U$ weighted mean age of 338 ± 2 Ma (MSWD = 0.91, n = 19) with a similar concordia age of 339 ± 2 Ma (Figure 9i).

Mount Darcy

Zircon grains from sample MD16 (Mount Darcy) are mostly euhedral and show weakly developed concentric zoning in CL images (Figure 8j). The analyses yield a $^{206}Pb/^{238}U$ weighted mean age of 375 ± 2 Ma (MSWD = 7.3, n = 25; Figure 9j).

Discussion

Timing of magmatism in the Georgetown region

New and published zircon U–Pb ages collectively define a Permian magmatic episode in the Georgetown region at *ca* 296–280 Ma. New ages for the Awring, Carnes and Mount Sircom intrusions and the Prestwood Granite cluster between 296 and 285 Ma, while a published age of 280 Ma for the Yataga Granodiorite extends this episode into the late Permian (Champion & Bultitude, 2013b).

Geochronological data define a broader Carboniferous magmatic episode in the Georgetown region at *ca* 360–330 Ma. This interval is constrained by our new ages for the Culba Granite (360 Ma) and Lochaber Granite (333 Ma), together with published emplacement ages for the Lochaber ring complex (351 and 338 Ma; Murgulov *et al*., 2009) and the Bousey Rhyolite (*ca* 330 Ma; Champion & Bultitude, 2013b). The Lochaber age also overlaps the published age of Kidston mineralisation (336 Ma; Murgulov *et al*., 2009).

The Mount Darcy intrusion was previously assigned to the KIA (reported at 330 Ma; Champion & Bultitude, 2013b), but it is a clear age outlier in our dataset (375 Ma) and pre-dates the KIA time window considered here (even allowing for an older

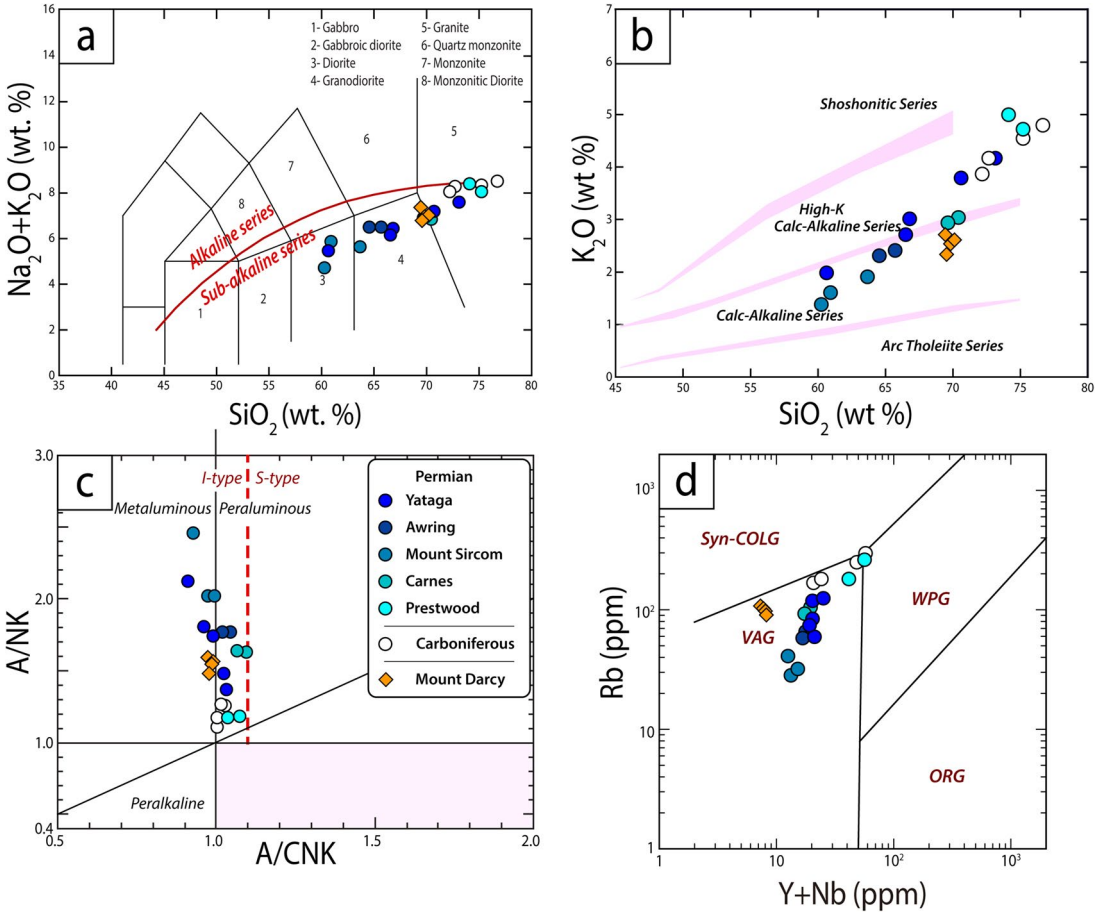


Figure 7. Geochemical classifications of the Permian group, Carboniferous group and Mount Darcy (symbols as in Figure 4). (a) Total alkali *vs* silica diagram (TAS) ($Na_2O + K_2O$ *vs* SiO_2 diagram) (Le Maitre *et al*., 1989). (b) K_2O *vs* SiO_2 diagram (Rickwood, 1989). (c) A/NK *vs* A/CNK diagram (Maniar & Piccoli, 1989). Dashed line is for A/CNK = 1.1. (d) Rb *vs* Y + Nb diagram (Pearce *et al*., 1984).

onset suggested by the Culba Granite at 360 Ma). Instead, its Devonian age is more consistent with magmatism and/or thermally reset age patterns attributed to the Pama Igneous Association in the Georgetown region, including K–Ar ages of 415–370 Ma reported for this study area (Morrison *et al*., 2019). We therefore interpret Mount Darcy as part of a late Pama magmatic episode rather than the KIA.

Implications of adakitic affinity

Adakitic geochemical characteristics of the Permian group

Adakitic affinity is commonly evaluated using high Sr/Y and La/Yb (or $(La/Yb)_N$) coupled with low Y and Yb, and routinely assessed on Sr/Y–Y and $(La/Yb)_N$ –Yb_N discrimination diagrams (Defant & Drummond, 1990; Moyen, 2009). Adakitic signatures have not previously been reported for granitoids in the Kidston subprovince; however, some KIA granitoids elsewhere show high Sr and Sr/Y and low Y and HREE, particularly in the Herberton, Burdekin Falls and Paluma subprovinces (Champion & Bultitude, 2013b). Although not all samples meet every criterion of 'classical' adakite definitions (*e.g.* Defant & Drummond, 1990; Martin *et al*., 2005), the Permian group from the Kidston subprovince is characterised by high Sr, Sr/Y and $(La/Yb)_N$ together with low Y and Yb. Classical adakites are typically low-K tonalitic to trondhjemitic rocks consistent with melting of a mafic source. In contrast, the comparatively potassic compositions of the Permian group were likely enhanced by K-enrichment during magmatic differentiation, as indicated by increasing K_2O and decreasing CaO and Sr with increasing SiO_2. A contribution from K-bearing components within a heterogeneous lower continental crustal source cannot, however, be excluded. On Sr/Y–Y and $(La/Yb)_N$–Yb_N discrimination diagrams, most Permian group samples plot within the adakitic fields, except for YTG06 (the most fractionated Yataga sample) and the Prestwood Granite (Figure 10a, b). Yataga samples have Na_2O contents at or slightly below the nominal threshold commonly cited for sodic adakites (>3.5 wt%). Nevertheless, the adakitic affinity of the Permian group is primarily expressed by the granodiorite–tonalite intrusions, which show low Y (7.2–16.5 ppm) and Yb (0.6–1.6 ppm) together with elevated Sr/Y and $(La/Yb)_N$. Although Mount Darcy also shows adakitic-like Sr/Y, it is treated separately as a pre-KIA outlier based on its *ca* 375 Ma zircon U–Pb age.

In contrast, the Carboniferous group has lower Sr (<250 ppm) and higher Y (12.6–39.5 ppm) and Yb (1.3–4.3 ppm) than the

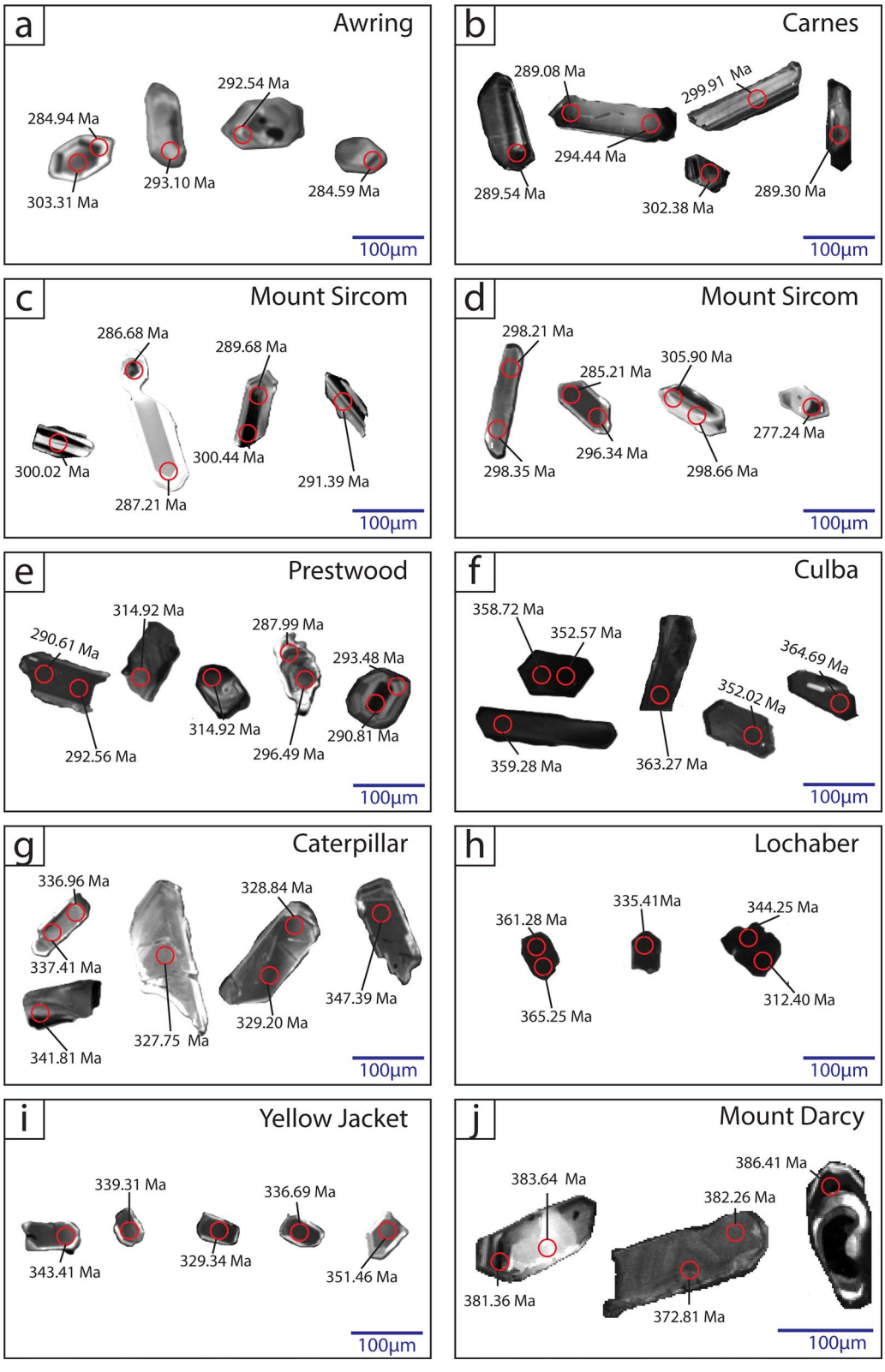


Figure 8. Cathodoluminescence (CL) images of representative zircon grains from the Permian group, Carboniferous group and Mount Darcy, with LA-ICP-MS spot locations (red circles) and corresponding $^{207}Pb/^{235}U$ apparent ages (Ma) shown for selected analyses. Scale bars = 100 µm. (a) Awring Granodiorite; (b) Carnes Granodiorite; (c–d) Mount Sircom Granodiorite; (e) Prestwood Granite; (f) Culba Granite; (g) Caterpillar Granite; (h) Lochaber Granite; (i) Yellow Jacket Rhyolite; (j) Mount Darcy Granodiorite.

Permian group, despite similarly sodic compositions (Na_2O = 3.70–4.17 wt%). Consequently, the Carboniferous group shows low Sr/Y and $(La/Yb)_N$ that fall below commonly used cutoff values, and these samples plot in the 'normal arc' fields rather than the adakitic fields (Figure 10a, b). Overall, the Permian group shows a stronger but variable adakitic affinity

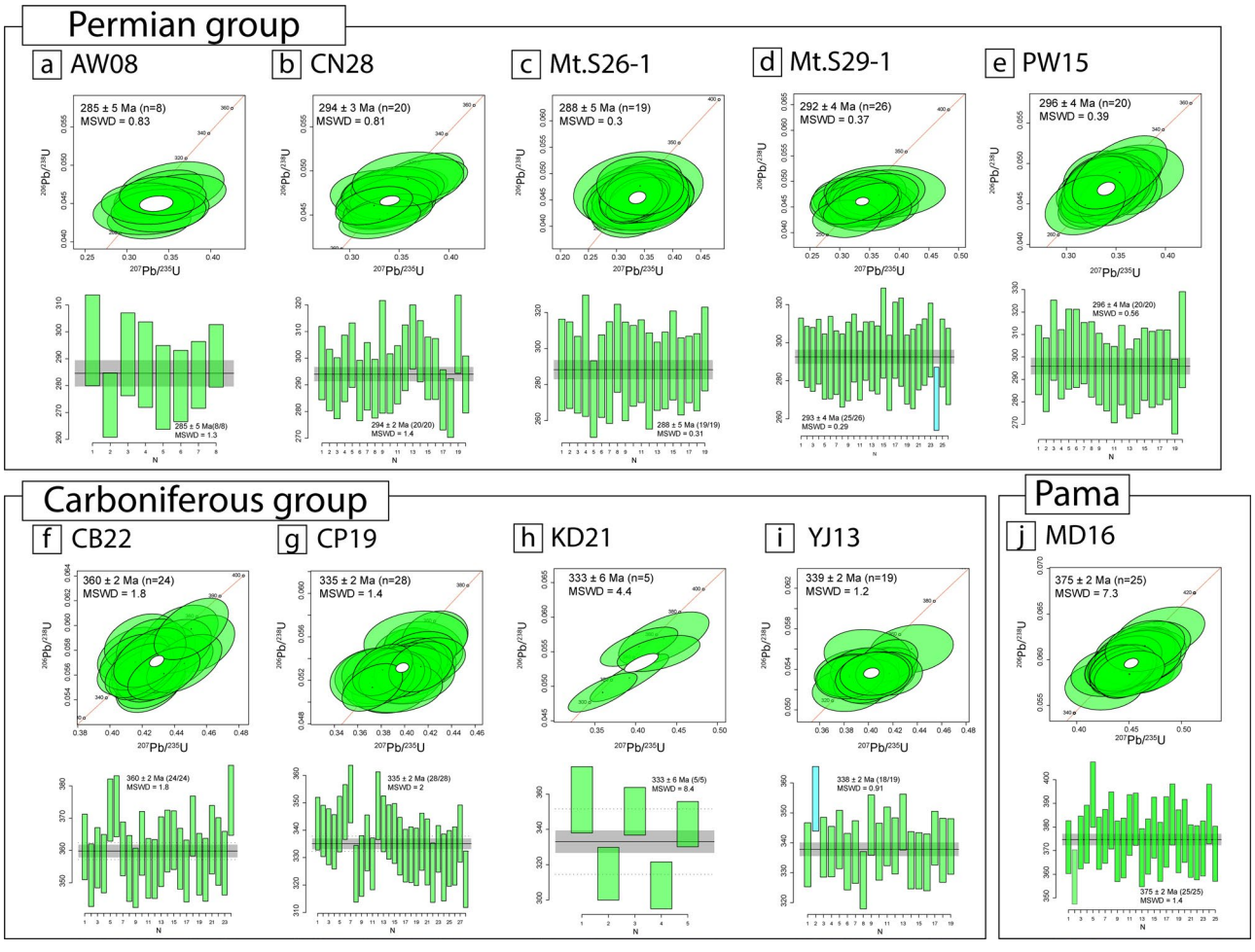


Figure 9. Wetherill U–Pb concordia diagrams (LA-ICP-MS) with corresponding $^{207}Pb/^{235}U$ apparent-age spectra for samples from the Permian group, Carboniferous group and Mount Darcy.

relative to the Carboniferous group, with the clearest expression occurring in the less evolved granodiorite–tonalite intrusions, whereas the Carboniferous group lacks these characteristics.

The Permian intrusions are not interpreted as products of a single magma chamber or as a strictly cogenetic suite. Rather, their overlapping emplacement ages and broadly similar geochemical characteristics suggest separate magma batches generated within a shared regional lower-crustal source framework. The strength of their adakitic affinity nevertheless varies with differentiation. The comparatively low-SiO_2 Mount Sircom granodiorites have the highest Sr and Sr/Y values and show weakly positive Eu anomalies (Figure 6a), consistent with limited removal, and possibly minor accumulation, of plagioclase. In contrast, the more evolved Permian units generally show decreasing CaO, Sr and Sr/Y, increasing K_2O, and progressively more negative Eu anomalies with increasing SiO_2. These covariations indicate that subsequent differentiation involving plagioclase fractionation progressively modified and weakened the initial high Sr/Y signature. Accordingly, the Permian intrusions are interpreted as sharing a broadly similar petrogenetic framework rather than displaying a uniform adakitic signature or constituting a single cogenetic differentiation series.

Constraints on the source of adakitic magmas in the Permian group

A potential relationship with low-silica adakite (LSA) magma was evaluated because high-silica adakitic rocks may, in some cases, represent differentiated derivatives of an LSA parental magma or felsic members of a cogenetic LSA–high-silica adakite suite (Moyen, 2009). Here, Mg# was calculated as 100 × molar Mg/(Mg + Fe), with total Fe_2O_3 converted to FeO prior to calculation. However, the Permian granodiorite–tonalite intrusions have generally low MgO contents (<3 wt%, except YTG01-1) and Mg# values (35–53), unlike the relatively magnesian compositions commonly associated with LSA magmas and their interaction with mantle material. Moreover, no cogenetic LSA or other mafic members have been documented in the Georgetown region. We therefore consider derivation from an LSA parental magma, or membership in a cogenetic LSA–high-silica adakite suite, unlikely. Magma mixing between mafic and felsic magmas is also unlikely given the low Mg# values (*cf.* high-Mg andesites with Mg# > 60; Streck *et al.*, 2007) and the absence of documented coeval mafic magmatism (*e.g. ca* 290 Ma basalts) in the Georgetown region. The distribution of the Permian samples in the La–La/Yb diagram is closer to the

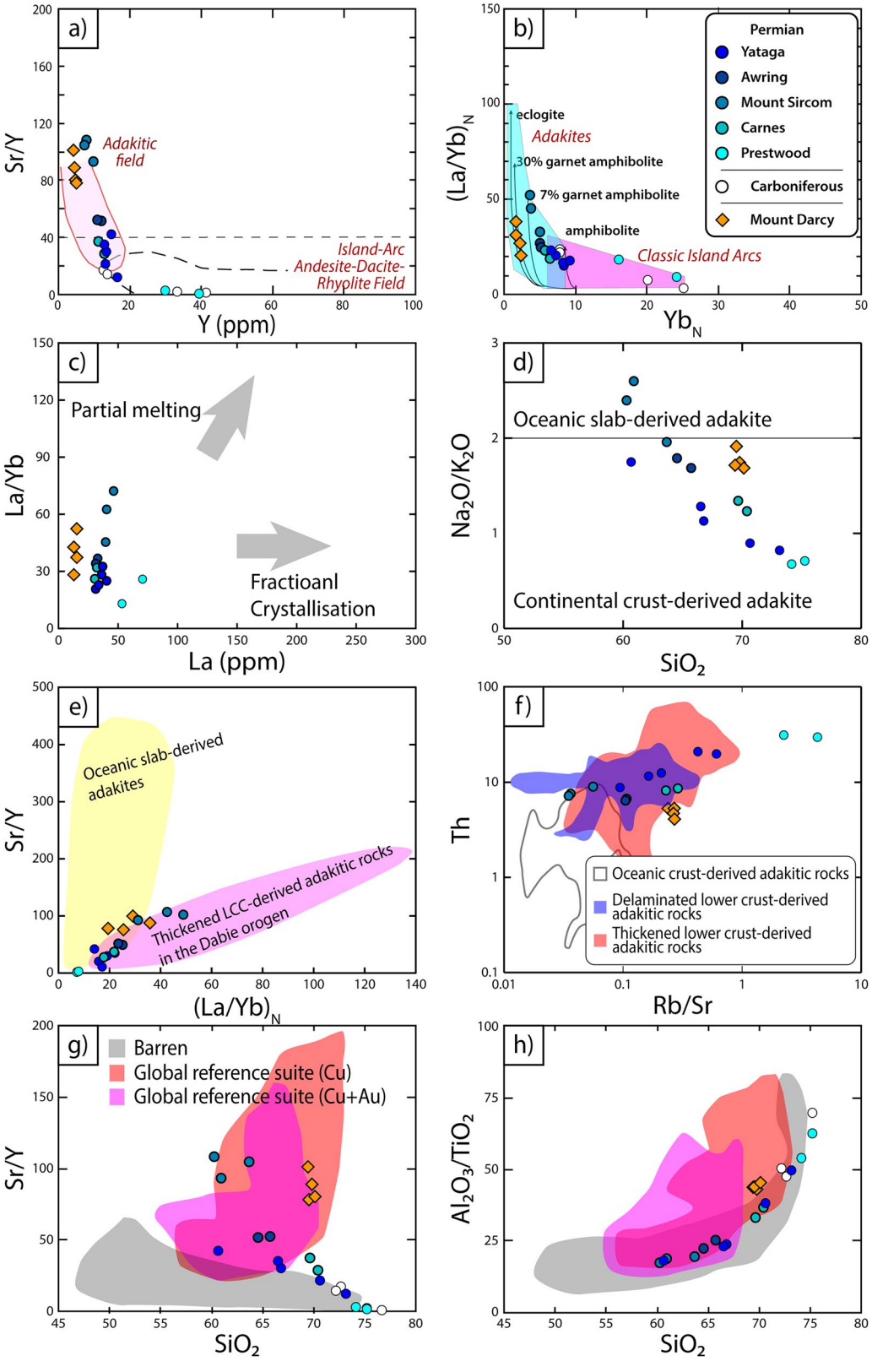


Figure 10. Whole-rock geochemical discrimination diagrams used to evaluate adakitic affinity for the Permian group (a–f) and Cu–Au fertility discrimination diagrams for Permian group, Carboniferous group and Mount Darcy (g, h) (symbols as in Figure 4). (a) Sr/Y *vs* Y. (b) $(La/Yb)_N$ *vs* Yb_N (Defant & Drummond, 1990), showing reference batch partial melting trajectories for mafic lower-crustal sources with amphibolitic, 7–30% garnet-bearing amphibolitic and eclogitic residues (modified after Petford & Atherton, 1996). (c) La/Yb *vs* La (Kawaguchi *et al*., 2023). (d) Na_2O/K_2O *vs* SiO_2 (Jia *et al*., 2016). (e) Sr/Y *vs* $(La/Yb)_N$ (Hu *et al*., 2015; Liu *et al*., 2010). (f) Th *vs* Rb/Sr (Kawaguchi *et al*., 2023). (g) Sr/Y *vs* SiO_2 (Loucks, 2014). (h) Al_2O_3/TiO_2 *vs* SiO_2 (Loucks, 2014).

partial-melting trend than to the fractional-crystallisation trend (Figure 10c; Kawaguchi *et al.*, 2023; Turner *et al.*, 1996), suggesting that their REE characteristics retain a significant source-melting contribution. However, this relationship does not independently exclude modification by subsequent fractional crystallisation. The relatively high Rb/Sr ratios nevertheless indicate that substantial fractional crystallisation affected the Permian magmas (Blevin, 2004). However, high Rb/Sr alone does not require assimilation, and the absence of documented coeval mafic magmatism and mafic xenoliths provides little evidence for an assimilation–fractional crystallisation (AFC) process involving mafic parental magmas. We therefore consider fractional crystallisation to have contributed to the compositional evolution of the Permian group, but not to have been the primary control on its adakitic affinity.

Oceanic slab-derived adakitic rocks commonly have lower K_2O (<3.2 wt%) and higher Na_2O/K_2O (>2) (Jia *et al.*, 2016; Martin *et al.*, 2005). In contrast, Permian granodiorite–tonalite intrusion samples have $Na_2O/K_2O < 2$ (Figure 10d) and plot predominantly within fields interpreted as lower continental crust-derived adakitic rocks (*e.g.* Tibet and Dabie; Hu *et al.*, 2015; Jia *et al.*, 2016), rather than oceanic slab-melt adakites (Figure 10e; Hu *et al.*, 2015; Liu *et al.*, 2010). The Permian group also shows relatively high Rb/Sr ratios and Th contents and overlaps the fields for thickened- and/or delaminated-lower-crust-derived adakitic rocks (Figure 10f). However, because Rb and Sr may be mobile during post-magmatic alteration, Rb/Sr is treated only as supporting evidence and is not used independently to determine magma source or petrogenetic process. Collectively, these geochemical features make partial melting of subducted oceanic crust unlikely; accordingly, a continental lower-crustal source is favoured over slab melting. The identification of Mesoproterozoic continental-arc basement beneath parts of northeastern Queensland demonstrates the presence of older continental crust that could have contributed to Paleozoic magma generation (Edgar *et al.*, 2025). However, its lower-crustal mineralogy is not sufficiently constrained to demonstrate a specific garnet-bearing, plagioclase-poor source. The high Sr/Y and low Y–Yb signatures require melting or differentiation under garnet ± amphibole-stable conditions with limited plagioclase control, whereas the potassic compositions additionally require K-bearing phases or a K-rich crustal component. We therefore infer a compositionally heterogeneous continental lower-crustal source, while recognising that its precise mineral assemblage cannot be resolved from the available data.

We evaluate continental lower-crustal melting models using REE systematics to infer the possible residual phases (garnet ± amphibole). Chondrite-normalised REE patterns show convex-downward MREE–HREE shapes and low Yb contents (0.6–1.6 ppm) (Figure 6a), consistent with partial melting with residual garnet ± amphibole (Kawaguchi *et al.*, 2023). To assess this interpretation graphically, published batch partial-melting trajectories for mafic lower-crustal sources with amphibolitic, 7% and 30% garnet-bearing amphibolitic, and eclogitic assemblages are projected onto the diagram (Figure 10b; Petford & Atherton, 1996). Most Permian samples plot closer to the amphibolite and 7% garnet amphibolite trajectories than to the 30% garnet amphibolite and eclogite models. Together with the tendency of the samples to plot closer to the partial-melting trend than to the fractional-crystallisation trend in Figure 10c, these relationships are consistent with a significant contribution from partial melting of an amphibolitic lower-crustal source containing subordinate residual garnet. However, neither diagram uniquely excludes deep amphibole- or garnet-controlled differentiation. Because the composition of the Georgetown lower crust is not independently constrained, these published trajectories provide first-order constraints on residual mineralogy rather than defining a unique source composition or precise degree of partial melting. The Permian granodiorite–tonalite intrusions are therefore consistent with melting of overthickened lower continental crust and/or delaminated mafic lower crust associated with mantle upwelling (Figure 11). However, delamination-related adakitic rocks commonly show higher concentrations of compatible elements (*e.g.* Ni, Cr), MgO and Mg# owing to interaction with mantle material during ascent (Gao *et al.*, 2004). In the Georgetown granodiorite–tonalite intrusions, Mg# values lie near the proposed thresholds (Mg# ~45–50; Duan *et al.*, 2015; Jia *et al.*, 2017; Wang *et al.*, 2016, 2017), and the samples overlap the fields for both thickened- and delaminated-crust models. Therefore, the relative contributions of lower-crustal thickening and delamination cannot be uniquely resolved from the available dataset. Nevertheless, partial melting of a heterogeneous continental lower-crustal source remains the preferred interpretation when the REE systematics are considered together with the major- and trace-element characteristics.

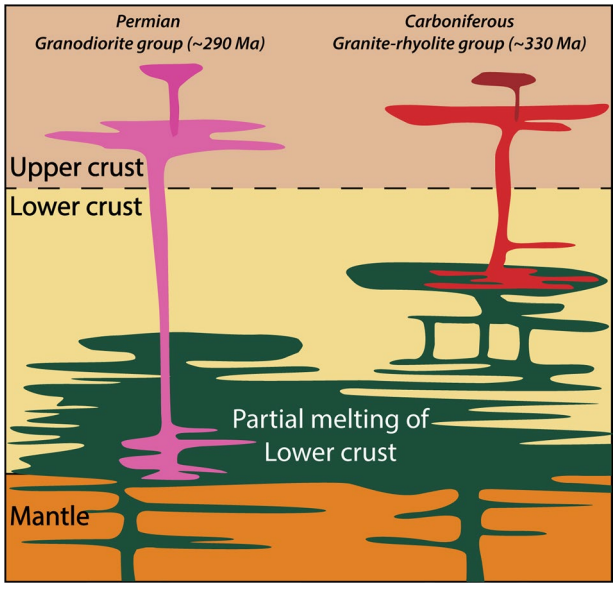


Figure 11. Conceptual cartoon illustrating contrasting magma sources and plumbing depths for Carboniferous and Permian magmatism in the Georgetown region (Kidston subprovince) (modified after Qu *et al.*, 2022). The Permian granodiorite–tonalite intrusions are interpreted to involve deeper crustal melt generation and/or storage, consistent with partial melting of lower crust under garnet ± amphibole-stable conditions. In contrast, Carboniferous magmatism is schematically shown as shallower crustal emplacement and storage, although the depth and source characteristics remain less well constrained. The dashed line marks the upper–lower crust boundary (not to scale).

Contrasting magmatism and tectonism along the eastern margin of Gondwana

The Permian–Carboniferous igneous rocks documented in this study provide new constraints on the tectono-magmatic evolution of northeastern Australia along the eastern margin of Gondwana. Zircon U–Pb ages indicate that magmatism in the Georgetown region was broadly coeval with intrusive activity in the adjacent Hodgkinson Province during the Carboniferous–Permian (*e.g.* Cheng *et al.*, 2018; Kumar *et al.*, 2022). However, whole-rock geochemical data reveal systematic differences in magma chemistry that require contrasting petrogenetic controls and imply along-strike variability in crustal architecture and magma evolution along this segment of the Gondwana margin.

The Permian group, especially its Permian granodiorite–tonalite intrusions, is characterised by elevated Sr/Y and $(La/Yb)_N$ ratios, low Y and Yb contents, and weak to absent Eu anomalies, indicating suppression of plagioclase fractionation and involvement of residual garnet ± amphibole during melt generation or early differentiation. These features are inconsistent with the shallow-crustal melting models previously proposed for Carboniferous–Permian granites of the Hodgkinson Province. Published zircon Hf-isotope and whole-rock geochemical data from the Hodgkinson Province have been interpreted to reflect mixed crustal–mantle sources and magma evolution at relatively low crustal pressures (Blevin, 2004; Blevin *et al.*, 1996; Cheng *et al.*, 2018). Instead, the Georgetown intrusions require magma generation and/or differentiation under higher-pressure conditions, consistent with partial melting of thickened lower continental crust or deep crustal magma storage.

Carboniferous–Permian magmatism in the Hodgkinson Province has been linked to long-lived subduction along the Gondwana margin, punctuated by tectonic switching, slab rollback and changes in magma oxidation state and fertility (Blevin, 2004; Blevin *et al.*, 1996; Cheng *et al.*, 2018). Within this framework, the adakitic affinity identified in the Georgetown Permian group represents a previously unrecognised magmatic component, implying localised deep crustal melting superimposed on the regional arc system. The presence of adakitic magmatism across the Hodgkinson–Georgetown inlier boundary supports a spatially heterogeneous arc evolution involving variable crustal thickness, magma storage depths and lithospheric modification rather than a laterally uniform continental arc. This regional evolution differs from the repeated S–I–A-type progression documented elsewhere in the Tasmanides (Collins *et al.*, 2020; Kemp *et al.*, 2009). In northeastern Queensland, increased A-type magmatism following predominantly I-type magmatism is consistent with slab-rollback-related extension, whereas younger S-type granitoids are largely restricted to the Mossman Orogen and likely reflect local involvement of sedimentary crust. These results refine existing models for Late Paleozoic magmatism in northeastern Australia and highlight the role of deep crustal processes in shaping the tectono-magmatic architecture of the Gondwana margin.

Metallogenic implications: Permian Cu–Au potential in the Georgetown region

Adakites and adakitic rocks with high Sr/Y have frequently been linked to magmatic–hydrothermal Cu–Au mineralisation and are widely used as geochemical indicators of porphyry fertility (*e.g.* Loucks, 2014; Sun *et al.*, 2011, 2012). In this study, the Permian group excluding the Prestwood Granite shows elevated Sr/Y and La/Yb and plots within (or close to) global reference fields associated with Cu(–Au) mineralisation. However, because most samples plot within the overlapping productive–barren reference fields, these diagrams alone cannot be used to confirm ore-forming fertility (Figure 10g, h). Despite this ambiguity, the combined high Sr/Y and La/Yb signatures are consistent with magmas that may have enhanced Cu–Au ore-forming potential.

Geochemically, the Permian group is best interpreted as continental adakitic magmatism generated by melting of the lower continental crust (Figure 10d–f). As discussed above, the available data do not uniquely distinguish between crustal thickening and delamination as the mechanism responsible for generating or remobilising this lower-crustal source. Although slab-melt adakites are commonly considered the most favourable end-member for large porphyry Cu–Au systems, ore-bearing continental adakitic rocks and Cu(–Au) deposits related to lower-crustal melting and/or delamination are documented in several regions (Hu *et al.*, 2015; Huang *et al.*, 2008; Li *et al.*, 2013; Wang *et al.*, 2007; Yang *et al.*, 2015). These examples indicate that continental adakitic magmatism can still be metallogenically significant, even where mantle input and/or lithospheric enrichment accompanies crustal melting.

In the Georgetown region, early Permian mineralisation is spatially associated with several intrusive and volcanic centres whose broadly constrained ages overlap the Permian group (Morrison *et al.*, 2019). Phyllis May is classified as an early Permian intrusion-related system associated with granodiorite, whereas Agate Creek mineralisation is hosted by rhyolitic sills dated at *ca* 285 Ma. In contrast, no direct age has been obtained for the intrusions or alteration at Huonfels, and its early Permian assignment is inferred from regional relationships with nearby dated intrusive and hydrothermal systems (Morrison *et al.*, 2019). These mineralised centres occur within or near the early Permian corridors shown in Figure 1b and display Au–Ag–base metal–Mo signatures and extensive alteration systems. However, comparable least-altered whole-rock major- and trace-element data are not currently available for the associated intrusions, and their Sr/Y, Y–Yb and REE characteristics therefore cannot be directly compared with those of the Permian group. Consequently, the spatial and temporal overlap and adakitic affinity of the Permian group identify these relationships as priorities for further testing rather than demonstrating a direct genetic association. Establishing such links will require direct constraints, including mineralisation ages, alteration and mineral chemistry and metal budgets, beyond whole-rock geochemistry alone. Although the Georgetown granitoids lack direct mineralisation constraints, the temporal overlap with regionally documented Permian Sn–Cu–In magmatic–hydrothermal systems (Kumar, Sanislav, Huang, *et al.*, 2024; Kumar, Sanislav, Martin *et al.*, 2024) suggests that similar oxidised, water-rich magmatic conditions may have prevailed, consistent with adakitic geochemical signatures.

Conclusions

This study combines whole-rock geochemistry with zircon U–Pb geochronology to constrain the timing, geochemical affinity and potential metallogenic significance of granitoids in the Georgetown region of northeastern Queensland. Zircon ages define two principal magmatic episodes: a Permian event represented by the Permian group (296–285 Ma), consistent with published ages for the Yataga Granodiorite, and an older Carboniferous episode represented by the Carboniferous group (360–333 Ma). The Prestwood Granite overlaps the Permian ages, whereas the Mount Darcy intrusion yields a Devonian age (*ca* 375 Ma) and is interpreted as part of a late Pama Igneous Association magmatic episode rather than the KIA.

Whole-rock major-element trends indicate broadly similar fractionation systematics in both groups (*e.g.* decreasing TiO_2, Al_2O_3, Fe_2O_3, MgO, CaO and P_2O_5 with increasing SiO_2), but the Permian group is relatively distinguished by higher Sr contents and REE patterns with stronger LREE–HREE fractionation and weak to absent Eu anomalies relative to the Carboniferous group. The Permian group, especially granodiorite–tonalite intrusions, also exhibits a consistent adakitic affinity, characterised by high Sr/Y and elevated $(La/Yb)_N$ coupled with low Y and Yb, and plots predominantly within adakitic fields on Sr/Y–Y and $(La/Yb)_N$ –Yb_N diagrams. In contrast, the Carboniferous group displays lower Sr and higher Y–Yb and lacks adakitic signatures. Petrogenetic constraints exclude LSA, mixing/AFC and slab-melt models, favouring a continental lower-crustal source. REE systematics are consistent with partial melting in the presence of residual garnet ± amphibole; however, the available dataset does not uniquely resolve whether lower-crustal thickening or delamination played the dominant role.

Although the Permian group is unlikely to represent slab-melt adakites associated with the largest porphyry Cu–Au systems, its adakitic affinity and Permian timing overlap with recognised mineralisation corridors in the Georgetown region. This indicates that the Permian group represents a prospective magmatic event that warrants further evaluation. Establishing direct genetic links to Cu–Au mineralisation will require additional constraints beyond whole-rock geochemistry, including mineralisation/alteration geochronology, mineral chemistry and quantitative metal budget indicators.

Acknowledgements

This study is part of a PhD project conducted by the first author, Jonghyun Lee, at JCU. The first author would like to acknowledge funding from Economic Geology Research Centre (EGRU) at JCU (Townsville, Australia). Hoseong Lim and Alexander Edgar are thanked for helping with fieldwork and sample collection and for being great colleagues.

CRediT authorship contribution statement

Jonghyun Lee: writing—original draft, visualisation, method, investigation, formal analysis, data curation, conceptualisation. Ioan V. Sanislav: writing—review and editing, validation, supervision, investigation, funding acquisition, conceptualisation. Helen A. Cocker: writing—review, visualisation—review and editing. Avish A. Kumar: writing—review and editing. Mabrouk. Sami: writing—review and editing, conceptualisation, resources, supervision.

Disclosure statement

No potential conflict of interest was reported by the authors.

ORCID

I. V. Sanislav http://orcid.org/0000-0002-3680-3740
H. A. Cocker http://orcid.org/0000-0002-5543-5701
J. Lee http://orcid.org/0009-0003-0592-4739

Data availability statement

Data are included within the paper and in the Supplemental data.

References

Atherton, M. P., & Petford, N. (1993). Generation of sodium-rich magmas from newly underplated basaltic crust. *Nature*, *362*(6416), 144–146. https://doi.org/10.1038/362144a0

Bain, J. H., & Draper, J. (1997). *North Queensland geology* (Vol. 240). Australian Geological Survey Organisation, Bulletin.

Baker, E. M., & Andrew, A. S. (1991). Geologic, fluid inclusion, and stable isotope studies of the gold-bearing breccia pipe at Kidston, Queensland, Australia. *Economic Geology*, *86*(4), 810–830. https://doi.org/10.2113/gsecongeo.86.4.810

Blevin, P., & Morrison, G. (1997). *Magmatic and hydrothermal evolution of major intrusive related gold deposits* Final Report, AMIRA project.

Blevin, P. L. (2004). Redox and compositional parameters for interpreting the granitoid metallogeny of eastern Australia: Implications for gold-rich ore systems. *Resource Geology*, *54*(3), 241–252. https://doi.org/10.1111/j.1751-3928.2004.tb00205.x

Blevin, P. L., Chappell, B. W., & Allen, C. M. (1996). Intrusive metallogenic provinces in eastern Australia based on granite source and composition. *Earth and Environmental Science Transactions of the Royal Society of Edinburgh*, *87*(1-2), 281–290. https://doi.org/10.1130/0-8137-2315-9.281

Bultitude, R., Garrad, P., Donchak, P., Domagala, J., Champion, D., Rees, I., Mackenzie, D., Wellman, P., Knutson, J., & Fanning, C. (1997). Cairns region. In J. H. C. Bain & J. J. Draper (Eds.), *North Queensland geology* (Vol. 240, pp. 225–325). Australian Geological Survey Organisation Bulletin.

Bultitude, R. J., & Champion, D. C. (1992). *Granites of the eastern Hodgkinson Province–their field and petrographic characteristics*. Geological Survey of Queensland Record 1992/06. https://geoscience.data.qld.gov.au/dataset/cr040898

Champion, D. C. (1994). *Igneous rocks of Northern Queensland: 1:5000,000 map and explanatory notes*. Australian Geological Survey Organization Record 1994/11. https://d28rz98at9flks.cloudfront.net/14721/Rec1994_011.pdf

Champion, D. C., & Bultitude, R. J. (2013a). The geochemical and SrNd isotopic characteristics of Paleozoic fractionated S-types granites of north Queensland: Implications for S-type granite petrogenesis. *Lithos*, *162-163*, 37–56. https://doi.org/10.1016/j.lithos.2012.11.022

Champion, D. C., & Bultitude, R. J. (2013b). Kennedy Igneous Association. In P. Jell (Ed.), *Geology of Queensland* (pp. 473–514). Geological Survey of Queensland. https://geoscience.data.qld.gov.au/data/report/cr145752

Cheng, Y., Spandler, C., Chang, Z., & Clarke, G. (2018). Volcanic–plutonic connections and metal fertility of highly evolved magma systems: A case study from the Herberton Sn–W–Mo Mineral Field, Queensland, Australia. *Earth and Planetary Science Letters*, *486*, 84–93. https://doi.org/10.1016/j.epsl.2018.01.012

Collins, W. J., Huang, H. Q., Bowden, P., & Kemp, A. I. S. (2020). Repeated S–I–A-type granite trilogy in the Lachlan Orogen and geochemical contrasts with A-type granites in Nigeria: Implications for petrogenesis and tectonic discrimination. In *Post-Archean granitic rocks: Petrogenetic processes and tectonic environments* (Vol. 491, pp. 53–76). Geological Society, London, Special Publications. https://doi.org/10.1144/SP491-2018-159

Defant, M. J., & Drummond, M. S. (1990). Derivation of some modern arc magmas by melting of young subducted lithosphere. *Nature*, *347*(6294), 662–665. https://doi.org/10.1038/347662a0

Dirks, H. N., Sanislav, I. V., & Sharib, A. S. A. (2021). Continuous convergence along the paleo-Pacific margin of Australia during the Early Paleozoic: Insights from the Running River Metamorphics, NE Queensland. *Lithos*, *398-399*, 106343. https://doi.org/10.1016/j.lithos.2021.106343

Duan, F., Li, Y., Wang, R., Ji, Z., Cheng, W., & Guo, X. (2015). Characteristics and geological significance of adakitic rocks of the Dulunhe granite in Toli, Western Junggar. *Journal of Mineralogy and Petrology*, *35*, 8–16. https://doi.org/10.19719/j.cnki.1001-6872.2015.04.002

Edgar, A., Sanislav, I. V., & Dirks, P. (2022). Tectonic setting and mineralisation potential of the Cowley Ophiolite Complex, north Queensland. *Australian Journal of Earth Sciences*, *69*(8), 1132–1148. https://doi.org/10.1080/08120099.2022.2086173

Edgar, A., Sanislav, I. V., & Dirks, P. (2023). The origin of mafic–ultramafic rocks and felsic plutons along the Clarke River suture zone: Implications for porphyry exploration in the northern Tasmanides. *Australian Journal of Earth Sciences*, *70*(8), 1123–1138. https://doi.org/10.1080/08120099.2023.2234964

Edgar, A., Sanislav, I. V., & Dirks, P. (2025). A Mesoproterozoic missing link between eastern Australia and China during the transition from Nuna to Rodinia? *Geoscience Frontiers*, *16*(3), 102017. https://doi.org/10.1016/j.gsf.2025.102017

Fanning, C. M. (1996). *SHRIMP U–Pb zircon dating for AMIRA project P425*. AMIRA report A95-640.

Fisher, C. M., Paton, C., Pearson, D. G., Sarkar, C., Luo, Y., Tersmette, D. B., & Chacko, T. (2017). Data reduction of laser ablation split-stream (LASS) analyses using newly developed features within iolite: With applications to Lu-Hf + U-Pb in detrital zircon and Sm-Nd + U-Pb in igneous monazite. *Geochemistry, Geophysics, Geosystems*, *18*(12), 4604–4622. https://doi.org/10.1002/2017GC007187

Gao, S., Rudnick, R. L., Yuan, H-L., Liu, X-M., Liu, Y-S., Xu, W-L., Ling, W-L., Ayers, J., Wang, X-C., & Wang, Q-H. (2004). Recycling lower continental crust in the North China craton. *Nature*, *432*(7019), 892–897. https://doi.org/10.1038/nature03162

Hedenquist, J. W., & Lowenstern, J. B. (1994). The role of magmas in the formation of hydrothermal ore deposits. *Nature*, *370*(6490), 519–527. https://doi.org/10.1038/370519a0

Horstwood, M. S. A., Košler, J., Gehrels, G., Jackson, S. E., McLean, N. M., Paton, C., Pearson, N. J., Sircombe, K., Sylvester, P., Vermeesch, P., Bowring, J. F., Condon, D. J., & Schoene, B. (2016). Community-derived standards for LA-ICP-MS U-(Th-) Pb geochronology–Uncertainty propagation, age interpretation and data reporting. *Geostandards and Geoanalytical Research*, *40*(3), 311–332. https://doi.org/10.1111/j.1751-908X.2016.00379.x

Hu, Y-b., Liu, J-q., Ling, M-x., Ding, W., Liu, Y., Zartman, R. E., Ma, X-f., Liu, D-y., Zhang, C-c., Sun, S-j., Zhang, L-p., Wu, K., & Sun, W-d. (2015). The formation of Qulong adakites and their relationship with porphyry copper deposit: Geochemical constraints. *Lithos*, *220-223*, 60–80. https://doi.org/10.1016/j.lithos.2014.12.025

Huang, F., Li, S., Dong, F., He, Y., & Chen, F. (2008). High-Mg adakitic rocks in the Dabie orogen, central China: Implications for foundering mechanism of lower continental crust. *Chemical Geology*, *255*(1-2), 1–13. https://doi.org/10.1016/j.chemgeo.2008.02.014

Jackson, S. E., Pearson, N. J., Griffin, W. L., & Belousova, E. A. (2004). The application of laser ablation-inductively coupled plasma-mass spectrometry to in situ U–Pb zircon geochronology. *Chemical Geology*, *211*(1-2), 47–69. https://doi.org/10.1016/j.chemgeo.2004.06.017

Jell, P. (Ed.) (2013). *Geology of Queensland*. Geological Survey of Queensland. https://geoscience.data.qld.gov.au/data/report/cr145752.

Jia, L., Mo, X., Santosh, M., Yang, Z., Yang, D., Dong, G., Wang, L., Wang, X., & Wu, X. (2016). Early Cretaceous continental delamination in the Yangtze Block: Evidence from high-Mg adakitic intrusions along the Tanlu fault, central Eastern China. *Journal of Asian Earth Sciences*, *127*, 152–169. https://doi.org/10.1016/j.jseaes.2016.06.001

Jia, Z., Chen, W., Sha, X., & Wang, J. (2017). Discovery of middle permian adakitic rocks in south Qilian area, gansu and implications for tectonics and Cu (Au) mineralization. *Geotectonica et Metallogenia*, *41*(1), 222–234.

Kawaguchi, K., Oh, C. W., & Jeong, J. W. (2023). Geochemistry, zircon UPb ages and LuHf isotopes of Triassic plutons in the eastern Gyeonggi Massif, Korean Peninsula: Magma genesis and geodynamic implications for East Asia. *Lithos*, *436-437*, 106955. https://doi.org/10.1016/j.lithos.2022.106955

Kemp, A., Hawkesworth, C. J., Collins, W., Gray, C., & Blevin, P. (2009). Isotopic evidence for rapid continental growth in an extensional accretionary orogen: The Tasmanides, eastern Australia. *Earth and Planetary Science Letters*, *284*(3-4), 455–466. https://doi.org/10.1016/j.epsl.2009.05.011

Kumar, A., Sanislav, I. V., Cathey, H. E., & Dirks, P. H. (2023). Geochemistry of indium in magmatic–hydrothermal tin and sulfide deposits of the Herberton Mineral Field, Australia. *Mineralium Deposita*, *58*(7), 1297–1316. https://doi.org/10.1007/s00126-023-01179-7

Kumar, A., Sanislav, I. V., & Dirks, P. H. (2022). The geological setting of the indium-rich Baal Gammon and Isabel Sn–Cu–Zn deposits in the Herberton Mineral Field, Queensland, Australia. *Ore Geology Reviews*, *149*, 105095. https://doi.org/10.1016/j.oregeorev.2022.105095

Kumar, A., Sanislav, I. V., Huang, H., & Dirks, P. H. (2024). Cassiterite trace element discrimination diagrams to facilitate critical mineral exploration. *Journal of Geochemical Exploration*, *264*, 107530. https://doi.org/10.1016/j.gexplo.2024.107530

Kumar, A., Sanislav, I., Martin, L., Aleshin, M., & Dirks, P. (2024). Genesis of copper mineralization in the polymetallic tin deposits from the Herberton Mineral Field, Queensland, Australia. *Mineralium Deposita*, *59*(2), 291–311. https://doi.org/10.1007/s00126-023-01209-4

Le Maitre, R., Bateman, P., Dudek, A., Keller, J., Lameyre, J., Le Bas, M., Sabine, P., Schmid, R., Sørensen, S., & Streckeisen, A. (1989). *A classification of igneous rocks and glossary of terms*. Blackwell Scientific Publications.

Li, X-H., Li, Z-X., Li, W-X., Wang, X-C., & Gao, Y. (2013). Revisiting the "C-type adakites" of the Lower Yangtze River Belt, central eastern China: In-situ zircon Hf–O isotope and geochemical constraints. *Chemical Geology*, *345*, 1–15. https://doi.org/10.1016/j.chemgeo.2013.02.024

Liu, S-A., Li, S., He, Y., & Huang, F. (2010). Geochemical contrasts between early Cretaceous ore-bearing and ore-barren high-Mg adakites in central-eastern China: Implications for petrogenesis and Cu–Au mineralization. *Geochimica et Cosmochimica Acta*, *74*(24), 7160–7178. https://doi.org/10.1016/j.gca.2010.09.003

Loucks, R. (2014). Distinctive composition of copper-ore-forming arc magmas. *Australian Journal of Earth Sciences*, *61*(1), 5–16. https://doi.org/10.1080/08120099.2013.865676

Mackenzie, D., & Wellman, P. (1997). Kennedy Province. In J. H. C. Bain & J. J. Draper (Eds.), *North Queensland geology* (Vol. 240, pp. 488–500). Australian Geological Survey Organisation Bulletin.

Maniar, P. D., & Piccoli, P. M. (1989). Tectonic discrimination of granitoids. *Geological Society of America Bulletin*, *101*(5), 635–643. https://doi.org/10.1130/0016-7606(1989)101%3C0635:TDOG%3E2.3.CO;2

Martin, H., Smithies, R., Rapp, R., Moyen, J-F., & Champion, D. (2005). An overview of adakite, tonalite–trondhjemite–granodiorite (TTG), and sanukitoid: Relationships and some implications for crustal evolution. *Lithos*, *79*(1-2), 1–24. https://doi.org/10.1016/j.lithos.2004.04.048

McDonough, W. F., & Sun, S-S. (1995). The composition of the Earth. *Chemical Geology*, *120*(3-4), 223–253. https://doi.org/10.1016/0009-2541(94)00140-4

Morrison, G., Mustard, H., Cody, A., Lisitsin, V., Beams, S. (2019). *Metallogenic study of the Georgetown, Forsayth and Gilberton Regions, North*

Queensland. Terra Search Pty Ltd Report TS 2019/025. https://geoscience.data.qld.gov.au/dataset/cr114062

Moyen, J-F. (2009). High Sr/Y and La/Yb ratios: The meaning of the "adakitic signature". *Lithos*, *112*(3-4), 556–574. https://doi.org/10.1016/j.lithos.2009.04.001

Murgulov, V., Beyer, E., Griffin, W. L., O'Reilly, S. Y., Walters, S. G., & Stephens, D. (2007). Crustal evolution in the Georgetown Inlier, North Queensland, Australia: A detrital zircon grain study. *Chemical Geology*, *245*(3-4), 198–218. https://doi.org/10.1016/j.chemgeo.2007.08.001

Murgulov, V., Griffin, W. L., & O'Reilly, S. Y. (2009). Temporal and genetic relationships between the Kidston gold-bearing Breccia Pipe and the Lochaber Ring Dyke Complex, North Queensland, Australia: Insights from in situ U–Pb and Hf-isotope analysis of zircon. *Mineralogy and Petrology*, *95*(1-2), 17–45. https://doi.org/10.1007/s00710-008-0020-7

Oversby, B. S., McKenzie, D. (1994). *Geology of late Palaeozoic ignimbrites and associated rocks in the Georgetown Region, northeastern Queensland*. Australian Geological Survey Organisation Record 1994/20. https://d28rz98at9flks.cloudfront.net/14774/Rec1994_020.pdf

Pearce, J. A., Harris, N. B., & Tindle, A. G. (1984). Trace element discrimination diagrams for the tectonic interpretation of granitic rocks. *Journal of Petrology*, *25*(4), 956–983. https://doi.org/10.1093/petrology/25.4.956

Petford, N., & Atherton, M. (1996). Na-rich partial melts from newly underplated basaltic crust: The Cordillera Blanca Batholith, Peru. *Journal of Petrology*, *37*(6), 1491–1521. https://doi.org/10.1093/petrology/37.6.1491

Qu, P., Niu, H-C., Weng, Q., Li, N-B., Zhao, Y., & Zhang, H-J. (2022). Apatite and zircon geochemistry for discriminating ore-forming intrusions in the Luming giant porphyry Mo deposit, Northeastern China. *Ore Geology Reviews*, *143*, 104771. https://doi.org/10.1016/j.oregeorev.2022.104771

Richards, J. P. (2011). Magmatic to hydrothermal metal fluxes in convergent and collided margins. *Ore Geology Reviews*, *40*(1), 1–26. https://doi.org/10.1016/j.oregeorev.2011.05.006

Rickwood, P. C. (1989). Boundary lines within petrologic diagrams which use oxides of major and minor elements. *Lithos*, *22*(4), 247–263. https://doi.org/10.1016/0024-4937(89)90028-5

Seedorff, E., Dilles, J. H., Proffett, J. M., Einaudi, M. T., Zurcher, L., Stavast, W. J., Johnson, D. A., & Barton, M. D. (2005). *Porphyry deposits: Characteristics and origin of hypogene features* (pp. 251–298). Society of Economic Geologists. https://doi.org/10.5382/AV100.10

Sillitoe, R. H. (2010). Porphyry copper systems. *Economic Geology*, *105*(1), 3–41. https://doi.org/10.2113/gsecongeo.105.1.3

Sláma, J., Košler, J., Condon, D. J., Crowley, J. L., Gerdes, A., Hanchar, J. M., Horstwood, M. S. A., Morris, G. A., Nasdala, L., Norberg, N., Schaltegger, U., Schoene, B., Tubrett, M. N., & Whitehouse, M. J. (2008). Plešovice zircon—A new natural reference material for U–Pb and Hf isotopic microanalysis. *Chemical Geology*, *249*(1-2), 1–35. https://doi.org/10.1016/j.chemgeo.2007.11.005

Streck, M. J., Leeman, W. P., & Chesley, J. (2007). High-magnesian andesite from Mount Shasta: A product of magma mixing and contamination, not a primitive mantle melt. *Geology*, *35*(4), 351–354. https://doi.org/10.1130/G23286A.1

Sun, S-S., & McDonough, W. F. (1989). Chemical and isotopic systematics of oceanic basalts: Implications for mantle composition and processes. *Geological Society, London, Special Publications*, *42*(1), 313–345. https://doi.org/10.1144/GSL.SP.1989.042.01.19

Sun, W., Ling, M., Ding, X., Chung, S-L., Yang, X-Y., & Fan, W. (2012). The genetic association of adakites and Cu–Au ore deposits': A reply. *International Geology Review*, *54*(3), 370–372. https://doi.org/10.1080/00206814.2011.580617

Sun, W., Zhang, H., Ling, M-X., Ding, X., Chung, S-L., Zhou, J., Yang, X-Y., & Fan, W. (2011). The genetic association of adakites and Cu–Au ore deposits. *International Geology Review*, *53*(5-6), 691–703. https://doi.org/10.1080/00206814.2010.507362

Turner, S., Arnaud, N., Liu, J., Rogers, N., Hawkesworth, C., Harris, N., Kelley, S., Van Calsteren, P., & Deng, W. (1996). Post-collision, shoshonitic volcanism on the Tibetan Plateau: Implications for convective thinning of the lithosphere and the source of ocean island basalts. *Journal of Petrology*, *37*(1), 45–71. https://doi.org/10.1093/petrology/37.1.45

Vermeesch, P. (2018). IsoplotR: A free and open toolbox for geochronology. *Geoscience Frontiers*, *9*(5), 1479–1493. https://doi.org/10.1016/j.gsf.2018.04.001

Wang, D., Luo, L., Tang, Y., Yin, F., Wang, B., & Wang, L. (2016). Zircon U–Pb dating and petrogenesis of Early Paleozoic adakites from the Niujingshan ophiolitic mélange in the Changning-Menglian suture zone and its geological implications. *Acta Petrologica Sinica*, *32*(8), 2317–2329.

Wang, J., Li, Y., Li, H., & Dong, P. (2017). Discovery of Early Permian intra-oceanic arc adakite in the Meilaotewula ophiolite, Inner Mongolia and its evolution model. *Acta Geologica Sinica*, *91*(8), 1776–1795.

Wang, Q., Wyman, D. A., Xu, J., Jian, P., Zhao, Z., Li, C., Xu, W., Ma, J., & He, B. (2007). Early Cretaceous adakitic granites in the Northern Dabie Complex, central China: Implications for partial melting and delamination of thickened lower crust. *Geochimica et Cosmochimica Acta*, *71*(10), 2609–2636. https://doi.org/10.1016/j.gca.2007.03.008

Wellman, P. (1992). A geological interpretation of the regional gravity and magnetic features of north Queensland. *Exploration Geophysics*, *23*(1), 417–422. https://doi.org/10.1071/EG992423

Wellman, P. (1995). *Interpretation of regional magnetic and gravity data in Cape York Peninsula, Queensland*. Australian Geological Survey Organisation Record 1995/45. https://d28rz98at9flks.cloudfront.net/14847/Rec1995_045.pdf

Wellman, P., Mackenzie, D., & Bain, J. (1994). Permian–Carboniferous magmatism in north Queensland: A new perspective. *Australian Geological Survey Organisation Research Newsletter*, *20*, 8–9. https://d28rz98at9flks.cloudfront.net/90415/ResearchNews_20_p008.pdf

Wiedenbeck, M., Allé, P., Corfu, F., Griffin, W. L., Meier, M., Oberli, F., Quadt, A. V., Roddick, J. C., & Spiegel, W. (1995). Three natural zircon standards for U–Th–Pb, Lu–Hf, trace element and REE analyses. *Geostandards Newsletter*, *19*(1), 1–23. https://doi.org/10.1111/j.1751-908X.1995.tb00147.x

Withnall, I., Mackenzie, D., Denaro, T., Bain, J., Oversby, B., Knutson, J., Donchak, P., Champion, D., Wellman, P., & Cruikshank, B. (1997). Georgetown region. In J. H. C. Bain & J. J. Draper (Eds.), *North Queensland geology* (Vol. 240, pp. 19–116). Australian Geological Survey Organisation Bulletin.

Withnall, I. W., & Henderson, R. A. (2012). Accretion on the long-lived continental margin of northeastern Australia. *Episodes*, *35*(1), 166–176. https://doi.org/10.18814/epiiugs/2012/v35i1/016

Yang, Z-M., Lu, Y-J., Hou, Z-Q., & Chang, Z-S. (2015). High-Mg diorite from Qulong in southern Tibet: Implications for the genesis of adakite-like intrusions and associated porphyry Cu deposits in collisional orogens. *Journal of Petrology*, *56*(2), 227–254. https://doi.org/10.1093/petrology/egu076